DISSERTATIONES
CHIMICAE
UNIVERSITATIS
TARTUENSIS
177

JÖRGEN METSIK

Preparation and stability of poly(3,4-ethylenedioxythiophene) thin films for transparent electrode applications

DISSERTATIONES CHIMICAE UNIVERSITATIS TARTUENSIS
177

DISSERTATIONES CHIMICAE UNIVERSITATIS TARTUENSIS
177

JÖRGEN METSIK

Preparation and stability of poly(3,4-ethylenedioxythiophene) thin films for transparent electrode applications

UNIVERSITY OF TARTU
Press

Institute of Chemistry, Faculty of Science and Technology, University of Tartu, Estonia

The dissertation was accepted for the commencement of the degree of Doctor of Philosophy in Chemistry on June 21, 2018 by the Scientific Council of the Institute of Chemistry, University of Tartu.

Supervisors: Assoc. Prof. Uno Mäeorg, PhD
Institute of Chemistry, University of Tartu, Estonia

Martin Timusk, PhD
Institute of Physics, University of Tartu, Estonia

Opponent: Prof. Dr. Amir Fahmi
Faculty of Technology and Bionics
Rhein-Waal University of Applied Sciences, Germany

Commencement: Chemicum, 14A Ravila Street, Tartu, at 12.15 on August 29th, 2018

This research was supported by:

- The institutional research funding project IUT20-17 of the Estonian Ministry of Education.
- The Estonian Centre of Excellence in Zero Energy and Resource Efficient Smart Buildings and Districts, ZEBE, grant 2014-2020.4.01.15-0016 funded by the European Regional Development Fund.
- The Graduate School of Functional materials and technologies receiving funding from the European Regional Development Fund in University of Tartu, Estonia.

ISSN 1406-0299
ISBN 978-9949-77-808-9 (print)
ISBN 978-9949-77-809-6 (pdf)

University of Tartu Press
www.tyk.ee

CONTENTS

LIST OF ORIGINAL PUBLICATIONS

I Metsik, J.; Saal, K.; Mäeorg, U.; Lõhmus, R.; Leinberg, S; Mändar, H.; Kodu, M.; Timusk, M. Growth of Poly(3,4-ethylenedioxythiophene) Films Prepared by Base-Inhibited Vapor Phase Polymerization. *J. Polym. Sci. Part B: Polym. Phys.* **2014**, *52*, 561–571.

II Metsik, J.; Timusk, M.; Šutka, A.; Mooste, M.; Tammeveski K.; Mäeorg, U. *In situ* investigation of poly(3,4-ethylenedioxythiophene) film growth during liquid phase deposition polymerization. *Thin Solid Films* **2018**, *653*, 274–283.

III Metsik, J.; Timusk, M.; Käämbre, T.; Mändar, H; Umalas, M.; Kuus, A.; Puust, L.; Utt, K.; Sildos, I.; Mäeorg, U. Stability of poly(3,4-ethylenedioxythiophene) thin films prepared by vapor phase polymerization. *Polym. Degrad. Stab.* **2016**, *126*, 170–178.

IV Šutka, A.; Timusk, M.; Metsik, J.; Ruža, J.; Knite, M.; Mäeorg, U. PEDOT Electrodes for Triboelectric Generator Devices. *Org. Electron.* **2017**, *51*, 446–451.

Author's contribution:

I Was responsible for PEDOT film preparation and performing resistance measurements. Participated in designing the experiments and analyzing the results. Wrote main part of the manuscript.

II Was responsible for PEDOT film preparation, performing resistance and transmittance measurements. Participated in designing the experiments and was mainly responsible for analyzing the results. Wrote main part of the manuscript.

III Was responsible for PEDOT film preparation and participated in performing resistance and transmittance measurements. Participated in designing the experiments and was mainly responsible for analyzing the results. Wrote main part of the manuscript.

IV Was responsible for PEDOT film preparation. Participated in analyzing the results and writing the manuscript.

ABBREVIATIONS

AC	alternating current
AFM	atomic force microscope
DC	direct current
EDOT	3,4-ethylenedioxythiophene
$Fe(Tos)_3$	iron(III) *p*-toluenesulfonate
ICP	intrinsically conducting polymer
IMT	insulator-to-metal transition
ITO	indium tin oxide
LED	light-emitting diode
LPDP	liquid phase deposition polymerization
NIR	near-infrared
oCVD	oxidative chemical vapor deposition
PEDOT	poly(3,4-ethylenedioxythiophene)
PEG	polyethylene glycol
PHC	poly(1,6-hexanediol-co-citric acid)
PPG	polypropylene glycol
PSS	polystyrene sulfonate
RH	relative humidity
RMS	root mean square
TENG	triboelectric nanogenerator
Tos	*p*-toluenesulfonate
UV	ultraviolet
Vis	visible
VPP	vapor phase polymerization
XPS	X-ray photoelectron spectroscopy

For indicating the type of counterion in PEDOT, notation PEDOT:counterion is used.

INTRODUCTION

Intrinsically conducting polymers (ICPs) have fascinated scientists since the end of 20th century. These materials have numerous potential applications, including general use as transparent electrodes and more specific applications in various electronic and optoelectronic devices, for energy storage and electricity production, in electrochromic devices and various sensors. However, the properties of ICPs must correspond to the performance requirements regarding specific applications. For example, for using an ICP film as a transparent electrode, it needs to conduct sufficiently electricity and simultaneously have necessary transmittance in the visible wavelength range. Furthermore, the stability of relevant properties is also crucial. Polyacetylene may have high conductivity, but still remains only a scientific curiosity without commercial applications, because the stability of the material is too low.

Poly(3,4-ethylenedioxythiophene) (PEDOT) is an ICP, which is generally known for its quite high conductivity, transparency and stability in ambient conditions. Still, although PEDOT has remarkable properties among ICPs, these are not sufficient for every application. There is a remarkable variety of PEDOT preparations methods, which all have their downsides and upsides. It is necessary to understand PEDOT preparation methods to have a better control over the properties of the polymer.

In this study, two different PEDOT film preparation methods are explored and the stability of PEDOT films is determined in different environments. PEDOT film performance as a triboelectric nanogenerator (TENG) working electrode and contact surface is assessed.

Paper I in this thesis focuses on base-inhibited vapor phase polymerization (VPP), which is a well-known method suitable for preparation of highly conductive PEDOT films. However, VPP is very sensitive to environmental conditions. Paper I focuses on optimization of VPP process and the use of *in situ* resistance measurements for investigating polymerization.

Paper II explores the possibilities of liquid phase deposition polymerization (LPDP), which is a relatively novel method for preparing PEDOT films. *In situ* resistance measurements are combined with *in situ* transmittance measurements to gain a more complete understanding of the polymerization process.

The aim of paper III is to study the stability of VPP PEDOT and investigate, which factors accelerate degradation of conductivity. Different gaseous environments will be used for this purpose and room temperature measurements are combined with accelerated aging at elevated temperatures.

The purpose of paper IV is to use PEDOT films in TENGs. Different PEDOT-based electrodes are compared to choose a suitable material for PEDOT-based TENG contact surface/working electrode.

The optimal preparation conditions of PEDOT film by VPP and LPDP were determined and PEDOT film conductance was the most stable in dry and dark environments. VPP PEDOT was the best choice for TENG contact surface/ working electrode.

1. LITERATURE OVERVIEW

1.1. Intrinsically conducting polymers

ICPs are organic polymers, which conduct electricity. A breakthrough in ICP research was reported in 1977 in papers describing conductivity increase of polyacetylene doped with halogens or AsF_5.[1,2] For this discovery A. J. Heeger, H. Shirakawa and A. G. MacDiarmid were honored with the Nobel Prize in Chemistry 23 years later. Although several conducting polymers (e.g., polyaniline, polypyrrole and polyacetylene) and their conductive properties were known before these reports, the dramatic increase in conductivity up to more than seven orders of magnitudes sparked a wider scientific interest in this research area.[3]

Several types of ICPs have been developed, which have in common a characteristic conjugated system in the polymer backbone. Some examples of important ICPs are depicted in **Figure 1**. Good conductivity is generally achieved, when the concentration of charge carriers is high (high doping level), effective conjugation lengths long and polymer highly ordered (well-aligned polymer chains in a crystalline arrangement). For inorganic semiconductor "doping" means insertion of neutral atoms, but for ICPs "doping" is reduction or oxidation of the polymer with incorporation of counterions for electroneutrality.[3] In an undoped state, ICPs are insulators or low-conductivity semiconductors, because the band gap is typically around few eV, which is significantly larger than thermal energy at room temperature (~0.025 eV).[4] Charge carriers are introduced into ICPs as solitons, polarons or bipolarons.[3] Solitons are states in the center of the band gap, which occur only in degenerate polymers and can be filled with one electron (neutral soliton), two electrons (negatively charged soliton) or be empty (positively charged soliton). A polaron forms when an electron is added to or removed from the conjugated chain, a chain deformation occurs as a result and one electronic level is moved to the band gap both from the valence and conductance band. In the case of an electron polaron (radical anion), an electron is added to a level drawn from the conductance band and for a hole polaron (radical cation), an electron is removed from the level drawn from the valence band. By combination of two polarons with the same charge, a spinless bipolaron (dication or dianion) forms.

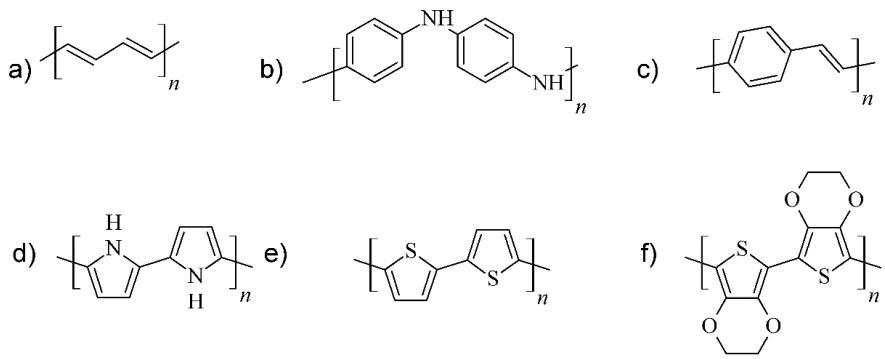

Figure 1. Important ICPs depicted in undoped state: a) *trans*-polyacetylene, b) polyaniline, c) poly(*p*-phenylene vinylene), d) polypyrrole, e) polythiophene, f) PEDOT.

Energetic barrier to motion of the charged species along the chain is small, but charge transport through a macroscopic sample is impeded by defects in the polymer chains and finite length of the chains.[4] Charge carrier motion in this kind of disordered materials is determined by hopping. Most of the ICPs behave as disordered semiconductors and conductivity reaches into metallic regime only for a few cases and even more rarely remains metallic at low temperatures.[4] In these cases, insulator-to-metal transition (IMT) can be observed. In an insulating (semiconducting) regime, conductivity could be generally described by hopping mechanism,[5] which has a following temperature dependence of conductivity:[6]

$$R(T) = R_0 \exp\left[\left(\frac{T_0}{T}\right)^{\alpha}\right] \tag{1}$$

T is temperature, R(T) temperature-dependent resistance, R_0 and T_0 material-dependent constants and α depends on dimensionality of transport (D), when variable-range hopping model is used:

$$\alpha = \frac{1}{1+D} \tag{2}$$

α=1 has been explained by nearest-neighbor hopping, while α=0.5 is consistent with an energy gap caused by Coloumb interactions between the carriers or charging-energy limited tunneling model.[7] α could be determined from the negative slope of log-log plots of reduced activation energy W as a function of T:[6]

$$W = -\frac{d(\ln R\,(T))}{d(\ln T)} \tag{3}$$

In the insulating (semiconducting) regime, W has a negative temperature coefficient; in the critical regime at the IMT, W is temperature independent for a wide range of temperatures and in the metallic regime, W has a positive temperature coefficient. Models describing transition to metallic conductivity regime need to take into account disorder in ICPs. The exact nature of IMT in ICPs has been controversial.[4,5] Two different possible models considered for ICPs are the Anderson disorder-induced transition or a percolation threshold for heterogeneously doped material. In the Anderson model, ICPs have a large homogeneously distributed disorder, which produces localized states and a mobility edge at the boundary between localized and delocalized states. At IMT, the Fermi level crosses the mobility edge. For heterogeneously doped material where highly doped metallic islands are separated by less conductive areas, reaching to percolation threshold at higher doping levels causes rapid increase in conductivity.

ICPs have rigid backbones, because a large amount of energy is required to disrupt the planarity of conjugated systems. Therefore, it is difficult to dissolve or melt these polymers, which results in poor processability.[4] Until the end of 1980s, usage of ICPs remained to be impractical due to insufficient stability of conductivity for known ICPs, but in the following decades polyaniline, polypyrrole and special polythiophenes found their way into the market.[3] PEDOT has played a considerable role in this development as the most successful and widely used polythiophene derivative.

1.2. Poly(3,4-ethylenedioxythiophene)

In the second half of 1980s, scientists at Bayer started to work with conducting polyheterocycles after initial failures to develop commercial products from other electrically conductive organic materials (e.g., polyacetylenes).[3] Although some polythiophenes exhibited a high conductivity, the instability of these materials in highly conductive form was problematic. Oxygen-substituted thiophenes were thought to stabilize the doped state. Although PEDOT was found to be insoluble, it had other remarkable properties like high conductivity (~300 S/cm), high stability in oxidized state and high transparency in thin oxidized films.[8] Unlike conducting polythiophenes PEDOT possessed remarkable stability against air humidity, which enabled to develop easily processable PEDOT suspension with polystyrene sulfonate (PSS) used initially as antistatic coatings.[3] PEDOT:PSS is prepared by oxidizing the monomer 3,4-ethylenedioxythiophene (EDOT) in the presence of PSS anions.

PEDOT could be prepared by chemical or electrochemical methods. The most widely used method is chemical oxidative polymerization (**Figure 2**), but there are also some additional methods like transition metal-mediated coupling of EDOT dihalogen derivatives and even spontaneous polymerization of 2,5-dibromo-EDOT.[3] Oxidative polymerization starts with the slowest step, EDOT oxidation to radical cation, which rapidly dimerizes. Endgroup oxidation is

remarkably faster for the dimer than the monomer. Finally, the polymer is oxidatively doped (**Figure 3**). Several oxidants could be used for chemical oxidative polymerization, including $FeCl_3$, MnO_2, $Ce(SO_4)_2$, $(NH_4)_2Ce(NO_3)_6$ and $CuCl_2$, while peroxodisulfates are a common choice for preparing PEDOT:PSS and iron(III) sulfonates suitable for making highly conductive PEDOT films.[3]

High conductivity of PEDOT is achieved by oxidizing the polymer and although it is possible to reductively dope PEDOT, it is impractical and results in instable conductivities.[8] About 1 in 3–5 monomeric units are usually oxidized in PEDOT:Tos and PEDOT:PSS films (doping level 20–35%).[9–12] However, for some systems extremely high doping values have been claimed in the literature, over 50%[13] and even up to ~90%[14]. Usually, the conductance in PEDOT systems (like PEDOT:PSS) is described by variable range hopping.[6] Although until recently, no metallic conductivity had been observed for PEDOT films,[3] several papers published in 2010s have reported that highly conductive PEDOT films are in the metallic conductance regime.[15–18] High conductivity in PEDOT has been associated with ordering of polymer chains, as evidenced by the ultrahigh conductivity values (~8000 S/cm) of PEDOT nanocrystals[19] or influence of film structuring additives on the growth of PEDOT films[16,20]. However, too bold generalizations about these complicated systems are frequently unwarranted. For PEDOT with moderately high conductivity values (600 S/cm), large changes in molecular ordering occurring during polymer washing did not improve the film conductivity at all.[21]

First commercially successful applications of PEDOT were its use in antistatic coatings and as a cathode material in solid electrolyte capacitors.[8] Later, a range of possibilities for PEDOT-containing devices has been studied, including electroluminescent lamps, organic light-emitting diodes, organic solar cells and field-effect transistors.[3] Furthermore, PEDOT is a promising material for replacing the most widely known transparent electrode material indium tin oxide (ITO). Compared to PEDOT, ITO is expensive and not compatible with flexible applications.[22] However, for replacing ITO PEDOT must have sufficiently high conductivity, transparency and stability.

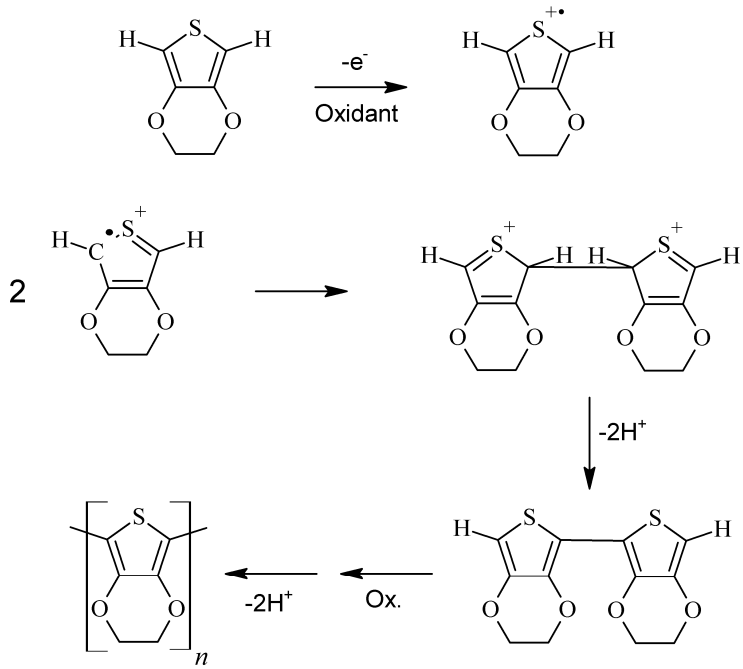

Figure 2. Chemical oxidative polymerization of EDOT. Oxidation of EDOT into radical cation is followed by $EDOT^+$ coupling into the EDOT dimer and subsequent similar coupling steps cause the formation of longer chains.[23]

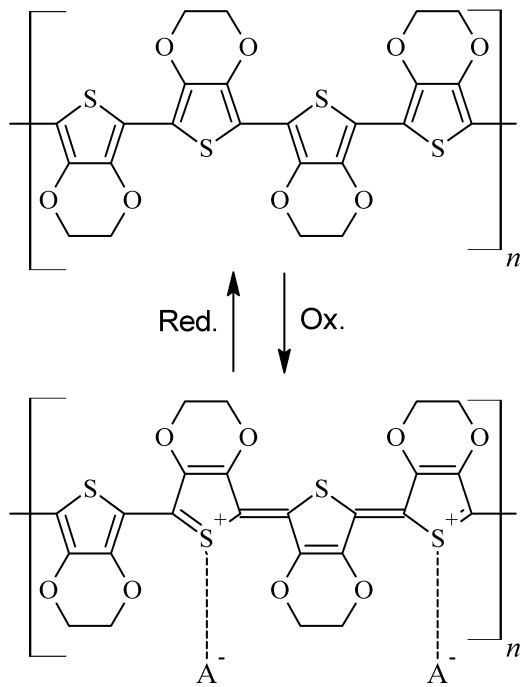

Figure 3. PEDOT could be in oxidatively doped (oxidized) or reduced (neutral) form.[23]

1.3. Preparation of PEDOT films

For PEDOT film preparation several methods based on electropolymerization and chemical oxidative polymerization are known. Typically, EDOT is electropolymerized in a three-electrode configuration in galvanostatic, potentiostatic or potentiodynamic mode.[24] PEDOT electropolymerizations are usually carried out in organic media,[24] but although EDOT has relatively low solubility in water, it could be electropolymerized in solvent-water mixtures or even in water.[8] Conductivities depend on used method and counterion, but values of 400–600 S/cm could be easily achieved.[8,10] It is possible to control the reaction by controlling the total charge passing through the electrode.[24] Still, electrochemical polymerization for PEDOT film preparation has some serious drawbacks as it is limited to conductive substrates and may produce non-uniform films for large areas[25] and uneven surfaces. By using chemical oxidative polymerization methods, virtually any surface could be covered with conductive PEDOT film.

PEDOT forms stable dispersions with PSS, which are commercially available and could be deposited by all common techniques employed for the deposition of waterborne coatings. Conductivity of PEDOT:PSS depends on PEDOT to PSS ratio, pH value (highest conductivities are in the pH range of 0 to 3) and the use of additional conductivity enhancing agents (so-called "second dopants"), e.g., ethylene glycol or dimethyl sulfoxide.[3] Effective second dopants are water-soluble additives with high dielectric constant and boiling point, which cause reorganization in the film structure and formation of highly conductive PEDOT-rich conduction path in the films. The best conductivity values of PEDOT:PSS films compare well to films prepared by other methods and conductivities up to 1000 S/cm could be routinely achieved by using commercially available PEDOT:PSS dispersions with the correct secondary dopant.[3] Furthermore, several methods enable to increase PEDOT conductivity to several thousands of S/cm, e.g., adding ionic liquid to PEDOT:PSS dispersion[26] or acid (e.g., sulfuric acid) treatment of prepared films[27]. Solution shearing and post-processing methanol treatment enabled to achieve sheet resistance (R_s) of 17 Ω/sq with 97% transmission at 550 nm and conductivity of 4600 S/cm.[22]

PEDOT films could be produced by directly mixing the oxidant (e.g., iron(III) *p*-toluenesulfonate, $Fe(Tos)_3$) and the monomer in a solvent (e.g., *n*-butanol) and casting the mixture on a substrate.[28] While $Fe(Tos)_3$ has good film-forming properties, the acidic environment of $Fe(Tos)_3$ solutions induces undesirable side reactions, likely including both formation of non-conjugated polymer and ether cleavage in the dioxane ring, which could be avoided by adding a basic inhibitor (e.g., pyridine).[28,29] The solution containing the monomer and the oxidant has a short pot-life of 10–20 minutes due to rapid polymerization and flocculate formation, causing difficulties in homogeneous film preparation, but pyridine additive enables to extend the pot-life to several days by slowing PEDOT formation reaction.[28] Polymerization is initiated by heating the monomer-containing oxidant films, which causes volatile pyridine

to slowly evaporate and desired polymerization reaction occurs only in a specific acidity range during evaporation of pyridine. This method enabled to achieve polymer film conductivities exceeding 1000 S/cm, surpassing the conductivities achieved by other known methods for PEDOT at the time of publication of these articles in years 2004–2005.[28,29] In addition to pyridine, other compounds, which are sufficiently basic and volatile, have been used for improving film conductivities. The conductivity-enhancing effect of basic inhibitors has been also explained by lowering the polymerization rate by decreasing the reactivity of Fe^{3+}.[30,31] Both basic properties and complexation with Fe^{3+} has been proposed to explain this rate-decelerating influence, although the exact mechanism is far from clear and inhibitors may influence polymerization also through several other factors.[30,32] As PEDOT films with very high conductivity have been later prepared with non-basic glycol copolymer inhibitors[20,33] and the influence of these inhibitors could partially be explained by slowing down reaction rate,[9,34] acid-initiated side-reactions do not seem to be an universal problem for this PEDOT preparation method. Imidazole and quinoline are suitable inhibitors for base-inhibited polymerization of EDOT, but due to the high boiling point of these compounds (257 °C[35] and 230 °C[28], respectively), it is inconvenient to evaporate these compounds, especially considering possible evaporation of EDOT (boiling point 190 °C), while pyridine with a lower boiling point of 115 °C is far more easily removed.[28] The relationship between acidity and conductivity of PEDOT films is complicated and acidic environment may enhance conductivity, if the film is exposed to acid after preparation. For PEDOT films prepared by spin-coating, a solution containing the monomer, iron(III) trifluoromethanesulfonate and a copolymer of polyethylene glycol (PEG) and polypropylene glycol (PPG) as an additive, subsequent treatment with *p*-toluenesulfonic, trifluoromethanesulfonic and sulfuric acid increased the conductivity, while hydrochloric and nitric acid decreased it.[15] Optimal results were gained with pH~1, pH below 0.5 caused degradation of the films. In 2016, PEDOT film conductivity of 3600 S/cm was achieved by a modification of the previously described synthesis technique involving addition of *N*-methyl-2-pyrrolidone as a cosolvent, while sulfuric acid treatment increased the film conductivity to an unprecedentedly high value of 5400 S/cm.[16] However, the practical value of acid treatment is likely somewhat limited, because acidic environments are frequently incompatible with practical applications of PEDOT films. The acidic and hygroscopic nature of PEDOT:PSS causes also instability of ITO/PEDOT:PSS interfaces,[36] which is one of the reasons for research in alternative PEDOT film preparation methods.

LPDP is a recently introduced polymerization method, which resembles VPP, but the source of the monomer is a liquid phase. A substrate covered with an oxidant layer is immersed into a monomer solution.[37,38] The oxidant film is poorly soluble in the solvent, which prevents the film from dissolving. This method enables to achieve better control over reaction environment compared to VPP, which depends on the distribution of monomer and water vapor in the chamber. Trichloromethane, cyclohexane and petroleum ether have been used

as solvents, while both $FeCl_3$ and $Fe(Tos)_3$ have served as oxidants.[37–39] Reported conductivities of LPDP PEDOT films are relatively modest (200–400 S/cm), but post-treatment in the oxidant solution increases the doping level and after post-treatment the conductivity may exceed 700 S/cm.[39]

1.4. Oxidative vapor deposition processes for PEDOT film preparation

Several methods utilizing the vapor phase for ICP deposition are known, including plasma-enhanced chemical vapor deposition, pulsed laser deposition, oxidative chemical vapor deposition (oCVD) and VPP.[31] For preparation of PEDOT films, oCVD and VPP are the most important of these techniques. oCVD of ICPs was first reported in 1986 by introducing pyrrole monomer vapor to $FeCl_3$ vapor under vacuum conditions.[40] oCVD of PEDOT was presented in 2006.[23] $FeCl_3$ was chosen as an oxidant, because $Fe(Tos)_3$ used frequently for VPP did not yield polymer films likely due to pyrolysis at high temperatures. oCVD does not depend on the wetting properties of a solution and therefore simplifies the coating process on a variety of organic and inorganic materials, being also suitable for coating high surface area morphologies, e.g., fibers and pores.[23] In a typical oCVD experiment, a substrate is placed inside a vacuum chamber onto an inverted temperature-controlled stage and $FeCl_3$ is sublimated from a heated crucible under the substrate, while the monomer is introduced at controlled flow rate from a heated vacuum system.[40] Use of bromine as an oCVD oxidant enabled to prepare PEDOT films in a completely dry process, avoiding not only the need to use solvent during preparation of the polymer film, but also washing the film to remove unreacted oxidant and undesirable by-products.[41] As an additional advantage, bromine is highly volatile, avoiding difficulties with uniform spatial delivery of oxidant, which complicate oCVD with $FeCl_3$.[40] However, bromine is highly corrosive and toxic. Although initially the conductivities of oCVD PEDOT films were limited to ~100 S/cm,[23] very high conductivities have been achieved later (~3500 S/cm)[42] by using $FeCl_3$ as an oxidant.

While during oCVD, both the oxidant and the monomer are delivered through the vapor phase, VPP (depicted in **Figure 4**) is a two-step process.[40] Initially, the substrate is covered with the oxidant solution, e.g., by spin-coating. The oxidant-treated substrate is subsequently inserted in a chamber containing monomer vapors, followed by washing the films with a suitable solvent to remove by-products and unreacted reactants. VPP takes place at the liquid-vapor interface[31] and although the oxidant films may appear to be dry prior to the experiment, the liquid-like state of oxidant films is necessary for film growth.[33] Without access to water vapor, no polymerization occurs in dried oxidant films, which was initially explained by water molecules possibly acting as proton scavengers in the deprotonation step of oxidative polymerization.[12,43] Later investigations revealed that the liquid-like behavior of the oxidant films

also allows the transport of the oxidant to the outermost surface of the film. This takes place *via* capillary action through a viscous liquid layer containing granular PEDOT particles, enabling film growth after the formation of the initial layer of PEDOT.[33] This conclusion was supported by X-ray photoelectron spectroscopy (XPS) results, which showed that even for oxidant-PEDOT films grown to a 150 nm thick PEDOT layer, iron species, including Fe^{3+}, were present at the topmost surface. VPP may be performed at ambient pressure, but vacuum conditions have been reported to increase the homogeneity of vapor distribution in the chamber, improving the homogeneity and reproducibility of the prepared PEDOT films.[44] Washing the film for by-product removal increases order in polymer chain alignment, but this effect does not seem to result in increased conductance.[21] However, conductivity depends mostly on reaching the percolation threshold for the unwashed film.

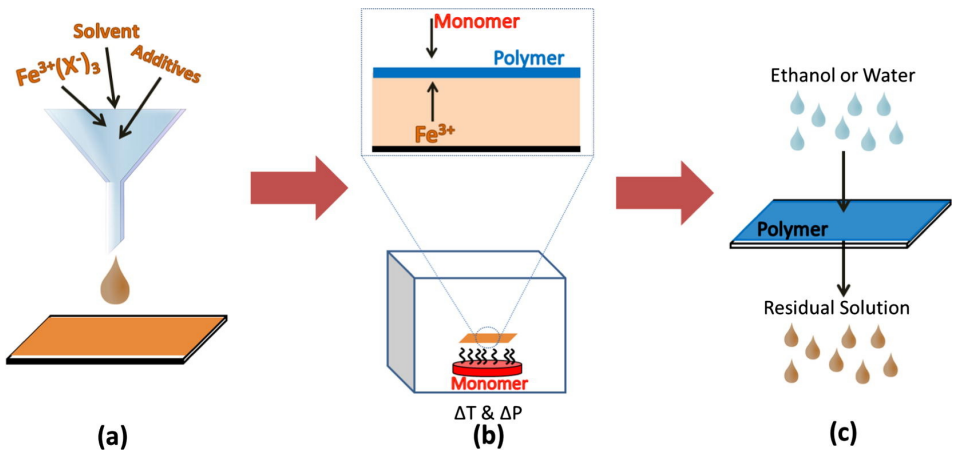

Figure 4. Schematic representation of general VPP procedure. a) Oxidant solution with necessary additives is cast onto a substrate, b) polymerization occurs at elevated temperature and frequently at lowered pressure in a special chamber and subsequently, c) the film is washed to remove unreacted oxidant and by-products.[31]

The conductivities of PEDOT films prepared by VPP using $FeCl_3$ oxidant were relatively low (~70 S/cm) when the method was initially applied for PEDOT film preparation.[45] Later, $Fe(Tos)_3$ has become a standard choice for preparing PEDOT by VPP. $Fe(Tos)_3$ oxidant gave superior VPP PEDOT films with more than ten times higher conductivity than using a variety of different Fe^{3+} salts containing chloride, camphor sulfonate, 4-ethylbenzenesulfonate and tetradecylsulfonate anions.[46] As attempts to exchange ions electrochemically did not influence the film conductivity, the authors proposed that different conductivities are caused by the ordering effect of the anion witnessed by a correlation between inter-chain stacking distance and conductivity. Interestingly, the degree

of ordered π-stacking did not influence the conductivity of the films. However, the claim remains controversial as effectiveness of the ion exchange was not proven and a later investigation has shown that ion exchange may take place only partially and even this kind of partial ion exchange actually influences the conductivity.[13] Ordered polymer forms only during washing the film without a large influence on base-inhibited VPP PEDOT conductivity.[21] $Fe(Tos)_3$ has been associated with higher conductivities than $FeCl_3$ oxidant due to lower effective oxidation strength and slower polymerization rate, which should give longer conjugation lengths and less defects in the polymeric material.[31] Using the $Fe(Tos)_3$ oxidant inhibited by pyridine enabled to increase the conductivities of VPP PEDOT films over 1000 S/cm.[28,29] In recent years it was demonstrated that iron(III) trifluoromethanesulfonate is also suitable for preparing very highly conductive PEDOT films.[15,16]

As an alternative to pyridine, different amphiphilic copolymers of PEG and PPG have been added to the oxidant solution for improving PEDOT film conductivity. Initially, it was demonstrated that adding PEG-*ran*-PPG copolymer enables to achieve similar conductivities to base-inhibited polymerization by suppressing oxidant crystal formation during water absorption from atmosphere in humid environments prior to polymerization.[25] Crystallized oxidant areas do not participate effectively in polymerization process, causing defect formation in the films. However, as water is necessary for film formation, presumably due to acting as proton scavenger during polymerization, it is not possible to obtain PEDOT films in completely water-free environments.[12,43] Also, PEG-*ran*-PPG was reported to decrease the growth rate of PEDOT films and extend the polymerization stage with slow growth rate, which allows to terminate polymer growth in a polymerization stage yielding high-conductivity films.[12,34] PEG-PPG-PEG copolymer forms complexes with the oxidant, increases the doping level and may also influence conjugation length and defects in the PEDOT backbone.[47] Further studies with tri-block PEG-PPG-PEG copolymers have claimed that the role of these additives in the EDOT polymerization process is even more complicated, improving water retention in the oxidant film[48] and maintaining liquid-like state of the oxidant layer in vacuum conditions with proposed simultaneous structure-directing effect on growing PEDOT.[33] The liquid-like state allows sufficient mobility of oxidant for film growth, while the hydrophilic and hydrophobic domains of amphiphilic copolymer cause redistribution of solution constituents according to their polarity resulting in structure-directing effect.[20] PEDOT thin film conductivity comparable to ITO (3400 S/cm) combined with a relatively low R_s (45 Ω/sq) and high transparency (transmittance >80% in the visible spectrum) has been achieved by optimizing the copolymer and solvent during the vacuum VPP.[20]

Fabretto et al. studied the PEDOT film growth process with $Fe(Tos)_3$ oxidant and PEG-*ran*-PPG additive using quartz crystal microbalance and AFM.[9] According to their results, PEDOT film grows in four stages. Initially, a first layer of PEDOT nodules forms. This step is dependent on the arrival rate of monomer and/or water vapor from the vapor phase. As the availability of the

exposed oxidant decreases when the PEDOT film starts to cover the oxidant surface, PEDOT growth rate slows down, marking the beginning of the second stage of polymerization. In the third stage, film growth rate accelerates again. For explanation, Fabretto et al. proposed initially that starting from the beginning of the second stage, the first step in the oxidative polymerization mechanism requires electron movement through the conductive polymer itself from the monomer to Fe^{3+}, as the oxidant is mostly covered by polymer surface.[9] Therefore, the polymerization rate decelerates compared to the first stage, as the number of conductive pathways to active oxidant sites is small. As percolation occurs in the film and more conductive pathways become available, the rate of polymerization accelerates again, marking the beginning of the third stage of polymerization. However, in a later study the same research group claimed that capillary transport of the viscous oxidant solution through the granular PEDOT layer enables polymerization by allowing the oxidant to directly contact with the monomer even in the later stages of film formation, which is contradictory to the previously proposed electron transport explanation.[33] Although the authors did not measure PEDOT growth rate in the second study, they showed that the amount of Fe^{3+} is extremely low at the surface in the early stages of PEDOT growth, but increases later, and proposed that the formation of a tight granular bed is necessary for initiating the capillary transport. The final stage of polymerization brings a decrease in polymerization rate, as the availability of oxidant becomes again limiting for the film growth.[9] The conductivity of PEDOT is high in the initial slow growth stages, but decreases at the start of the rapid third stage, which may be caused by different doping levels (higher in the beginning of polymerization) and possibly also more defective PEDOT chains with smaller conjugation lengths, which are less orderly aligned.[9] Although increasing doping levels may result in higher charge carrier densities and increased conductivity, the relationship between doping and conductivity is more complicated as excessive doping is associated with lower conductivity. Too high ratio of $Fe(Tos)_3$ to monomer leads to lower conductivity and transparency of PEDOT, presumably generating overdoped films containing immobilized charge carriers.[30]

1.5. Stability of PEDOT thin films prepared by oxidative vapor deposition processes

The stability of ICPs is an important factor limiting the potential applications of these materials. ICPs are used only sparingly in commercial devices, which could be explained to a large degree by stability issues, e.g., degradation in air and thermal decomposition at elevated temperatures.[31] Winther-Jensen and West determined that the conductivity of VPP PEDOT films slowly decreases and drops to a stable plateau value during one year, while similar changes occur almost instantaneously in water.[49] While initially PEDOT films had relatively high conductivities around 500–1000 S/cm, the new stable values of con-

ductivity were less than half of the initial values. However, the changes were largely reversible by immersing the aged films into *p*-toluenesulfonic acid solution, which increased conductivities almost to the initial values after aging. Winther-Jensen and West determined that film conductance is dependent on pH and decreases after immersing the PEDOT film into a basic solution and increases after immersing the film into acidic solution. The reversible nature of these changes indicated that no damage is done to the polymer backbones, but changes occur in the doping level, which was additionally indicated by changes in the bipolaron band in near-infrared (NIR) absorbance spectra. Although the reversibility of aging effects in acidic solutions is useful concerning PEDOT applications in aqueous environments, for most other applications this kind of treatment is not a practical possibility for avoiding aging-related degradation. Madl et al. obtained somewhat contradictory results to Winther-Jensen and West by observing that the conductivity of a VPP PEDOT film decreased for the first week, but was relatively stable for a following period of 50 days of storage in air.[50] Compared to VPP PEDOT, PEDOT:PSS and PEDOT prepared *in situ* from a solution were more stable according to Madl et al., but had significantly lower conductivities.

The conductivity of oCVD PEDOT prepared by using $FeCl_3$ or Br_2 decreased exponentially during accelerated aging experiments.[41] The stability of these PEDOT films was quite low at 100 °C, although the PEDOT films prepared by using Br_2 aged significantly slower. The lifetime of conductivity was in these conditions ~2000 s for PEDOT:Cl, but ~10 000 s for PEDOT:Br. In a later study, degradation of PEDOT:Cl films prepared by oCVD was associated with $FeCl_3$ impurity remaining in the film even after washing the films with methanol.[14] This impurity causes dedoping and a decrease in charge carrier density, which was determined by AC Hall effect measurements. Treatment of oCVD PEDOT:Cl films with aqueous solutions of some acids (HBr, H_2SO_4) does not only increase conductivity, but also increases stability.[14,51] It is still necessary to consider that for standard VPP PEDOT:Tos films the stability results of oCVD PEDOT:Cl may not apply, as the used oxidant and dopant anion are different.

1.6. Triboelectric nanogenerators

The working principle of TENGs was first demonstrated in 2012.[52] In these devices, two different materials are brought into contact with each other by external force and the surfaces of these materials obtain static charges. The contacting surfaces may be dielectric films prepared onto electrode materials that are connected by an external circuit. Alternatively, one of the surfaces may be a conductor, being both the triboelectric layer and the electrode.[53] Separating the oppositely charged surfaces generates an electric potential difference, which could be used for driving a current in an external circuit. To balance the

potential difference, charges flow from one electrode to another during the release. Bringing the surfaces again into contact will generate an opposite current flow; therefore, periodic switching will generate an output consisting of alternating current (AC) pulses.

Contact charging at conducting polymer interfaces may involve several different processes.[54] In the case of metal-metal or metal-semiconductor interfaces with zero or small band gaps, electron donor-receptor behavior is responsible for the acquired charge polarity and electrons flow until the equilibration of Fermi levels, but analogous processes require a large activation energy in dielectrics and for contact charging there is generally neither accepted theoretical basis nor definite relationship to some simple parameter (e.g., conductivity or dielectric constant).[55] Contact charge formation on organic polymers could be described by so-called triboelectric series, which lists the materials in the order of relative contact charge polarity starting from the material with the highest propensity to charge positively to the material, which has the highest propensity for negative charge accumulation.[56] Baytekin et al. investigated surface charging with Kelvin force microscopy and discovered that oppositely charged mosaic patterns form on polymer surfaces during contact electrification, which mostly compensate each other and only a slight excess of one type of charged micro-patterns determines the overall charge.[57] This indicates that surface charging is not a simple function of material composition. Still, Diaz and Felix-Navarro noticed that although contact charge formation in polymers is sensitive to numerous parameters (e.g., surface composition, surface characteristics, contact pressure, nature of the contact, relative humidity), nitrogen-containing polymers obtain highly positive charge, halogenated polymers highly negative charge and hydrocarbons almost no charge, while oxygen-containing polymers tend to charge slightly positively.[56] These effects were related to acid-base properties of the polymers, as polymers with basic properties had a tendency to charge positively, indicating water dissociation and transfer of resulting ions as the main contact charging mechanism. Heterolytic bond breakage may also have a role in contact charge formation.[57] However, it is still controversial to what extent the insulator surface charging results from the transfer of ions, because there is also evidence supporting electron transfer.[55] Additionally, for some softer materials so-called mass transfer may take place and charged species are transferred with minute amounts of polymeric material.[57,58]

TENGs could function in four fundamental working modes: vertical contact-separation mode, contact-sliding mode, single-electrode mode and freestanding triboelectric layer mode (**Figure 5**).[59] The simplest mode of vertical contact-separation has two dissimilar films (at least one of the films is an insulator) separated by a gap, which are tapped together during device operation. The contact of the surfaces creates opposite charges and once the two surfaces are again separated by a gap, a potential difference is created between electrodes and current flows through external load to balance the electrostatic field. After closing the gap, the triboelectric-charge-created potential disappears and the electrons flow back. Periodically repeating the procedure creates an AC output.

In the lateral sliding mode, triboelectric charges are created by relative sliding of the surfaces in parallel of the interface. A potential difference is generated by uncompensated charges in mismatched areas of periodically sliding electrodes. Sliding generates triboelectric charge more efficiently than vertical contact. In single-electrode mode, an electrically grounded electrode is in periodic contact with an insulating surface, developing contact charges and potential difference due to some kind of periodic movement (sliding or vertical contact-separation) between these two surfaces. The current is generated by electrons moving between the electrode and the ground. This design enables to harvest energy from an arbitrary freely moving object, but electrostatic screening limits its effectiveness. For the freestanding triboelectric layer mode, a pair of symmetric electrodes underneath a charged dielectric layer is separated by a gap and the cyclically moving dielectric layer generates potential difference by induction. This mode is known for its effectiveness and robustness.

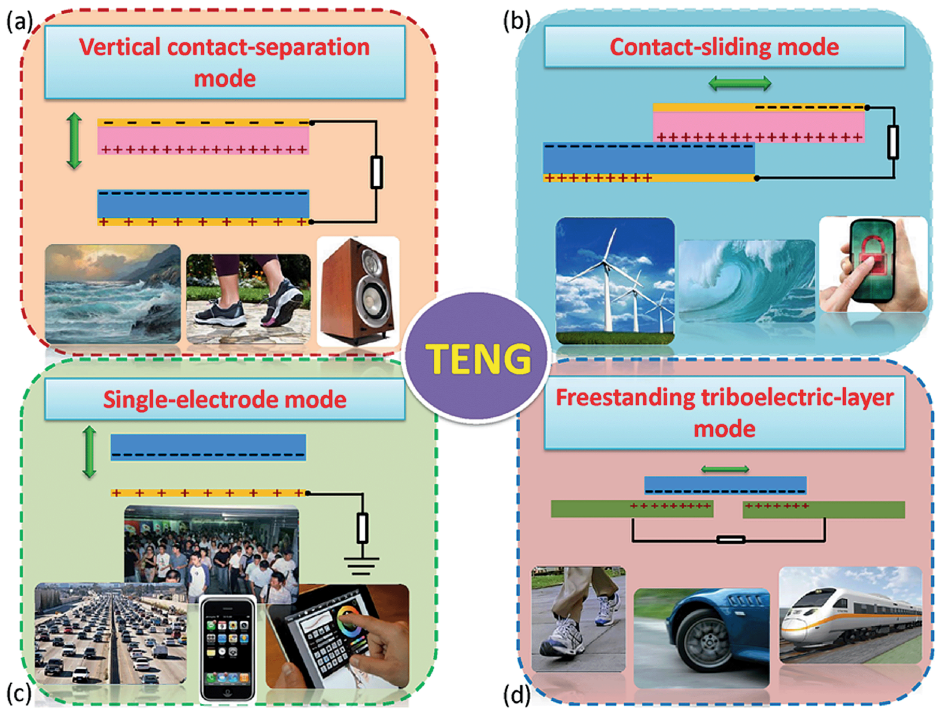

Figure 5. Working modes of a TENG are a) vertical contact-separation mode, b) contact-sliding mode, c) single-electrode mode and d) freestanding triboelectric layer mode.[60]

TENGs have potential applications for harvesting mechanical energy wasted in daily life and using it to power mobile self-powered devices, including bio-mechanical devices (e.g., pacemakers) and active sensors (pressure, motion, vibration, chemical and biomedical sensors), but also electricity production at a larger scale (wave and wind energy).[59] TENGs have high output power, could be prepared by scalable preparation process, are lightweight and require only small quantities of materials, which are all easily available.[61] Area power densities of 500 W/m^2, volume power densities of 15 MW/m^3 and instantaneous energy conversion efficiencies ~70% have been achieved.[59] Unfortunately, there are still some problems with practical applications of TENGs, mainly the mis-match of impedance between TENGs (high voltage, low current) and electronic devices (low voltage, high current), and also mechanical wear of polymer materials used for preparation of TENGs.[61]

2. AIMS OF THE STUDY

General aim of the present study was to investigate PEDOT preparation conditions and film properties relevant for the application of PEDOT films as transparent conductive electrodes. Potential practical applications of conductive polymer films as transparent electrode materials depend on several parameters of the films (e.g., conductivity, optical transmittance and stability of conductivity). For controlling film conductivity and transmittance, it is necessary to understand PEDOT film formation and growth better, which is the wider purpose of this study. Different PEDOT preparation methods based on chemical oxidative polymerization were in the focus of this study: VPP as a well-known PEDOT preparation method and LPDP as a relatively recently developed technique. These methods were investigated by rarely used *in situ* measurement techniques.

The other focus of research was the stability of PEDOT film conductivity as sufficient stability of the material in the working environment is crucial for any potential application. Therefore, investigating PEDOT stability in various environments is an important basis to determine potential uses of PEDOT electrodes. Moreover, testing potential applications of PEDOT electrodes was among the purposes of the study. The specific aims of the study were the following:

1. Investigating the influence of PEDOT preparation conditions during base-inhibited VPP on conductance and transmittance of the material for preparing PEDOT films with optimal properties (paper I).
2. Comparing PEDOT preparation by base-inhibited VPP with preparation by LPDP as an alternative method of chemical oxidative polymerization (paper II).
3. Investigating the stability of PEDOT thin film conductance in different gaseous environments, at different temperatures and in dark and UV-illuminated conditions (paper III).
4. Characterizing the PEDOT electrode as a replacement for the ITO electrode in TENGs (paper IV). Prepared VPP PEDOT films were suitable as a replacement for ITO contact surface/working electrode in TENGs.

3. METHODS

3.1. Preparation of substrates

Several different types of substrates were used for preparing PEDOT films. Amorphous silicon-titanium mixed oxide-coated glass substrates were chosen for optimizing the reaction time and temperature, because this oxide is used in liquid crystal-xerogel composite electro-optical films, making the surface properties of substrates comparable to these films. Silicon-titanium mixed oxide coated glass substrates were prepared using sol-gel method from tetraethylorthosilicate and titanium isopropoxide. The specific details are given in the published article.[62]

For monitoring electrical resistance during film growth and aging, a glass substrate patterned with highly conducting electrode film of Pt or ITO was used, which had a square-shaped glass surface in the center of the substrate surface surrounded by two rectangular substrate areas covered with highly conductive electrode films. For preparing TENG PEDOT electrodes, glass substrates with an ITO electrode strip in the edge were used for better electrical contact.

For preparing glass substrates with patterned ITO electrodes, ITO-covered glass substrates (R_s = 15 Ω/sq) were initially partially covered with Scotch tape. Subsequently, these substrates were repeatedly etched with concentrated hydrochloric acid (36.5–38%) and washed with deionized water, until the acid-exposed surface was non-conductive (up to a range of GΩ) and no ITO could be visually detected in the etched area. This method allowed to prepare a square-shaped ITO-free surface between ITO-electrodes on rectangular substrates (25 mm × 12.5 mm).

Pt-patterned electrodes were grown by sputter coating (Quorum Technologies SC7640 Sputter Coater) of platinum onto glass substrates, which were cut from microscope glass slides. A square-shaped area at the center of the substrate was covered with tape prior to sputter coating and rectangular Pt-electrodes were deposited onto the exposed area. The electrodes were annealed at 550–600 °C and had R_s values below 15 Ω/sq.

3.2. Preparation of PEDOT films

Preparation of PEDOT films by VPP comprised of several steps. Firstly, oxidant films were prepared onto substrates by spin-coating $Fe(Tos)_3$ solutions in *n*-butanol with a pyridine additive at 3000 rpm for 12 s. For *in situ* resistance measurements, a few mm wide strip on the measurement electrode was also covered with the oxidant solution to ensure electrical contact between polymer film and electrodes (inset in **Figure 6**). Solutions contained $Fe(Tos)_3$ and pyridine in a mass ratio of 25:1. Generally, 16% $Fe(Tos)_3$ solution by weight was used, if not claimed otherwise. After spin-coating, the films were dried in an oven at 80 °C for two minutes and inserted into a polymerization chamber

(**Figure 6**) placed on top of a temperature-controlled hot-plate at an elevated temperature. The polymerization chamber consisted of an 8 L glass dome hermetically sealed to an aluminum bottom with a stainless steel rim, equipped with air inlet valves used for pumping in air with specific relative humidity for humidity experiments, a relative humidity sensor (Honeywell HIH-4000-001) calibrated with saturated salt solutions and a Pt100 thermoresistor connected to Keithley 2400 sourcemeter for precise humidity and temperature measurements in air near the substrates. A drop of EDOT was inserted on a glass slide into the chamber. Polymerization was initiated by condensation of monomer vapors onto the substrates. Different polymerization temperatures, growth times and relative humidities were used for preparing the films. For some films prepared on Pt-patterned electrodes, electrical resistance was measured during film growth. The freshly polymerized films were washed with methanol for obtaining pure polymer films and removing unreacted oxidant, pyridine and reaction by-products.

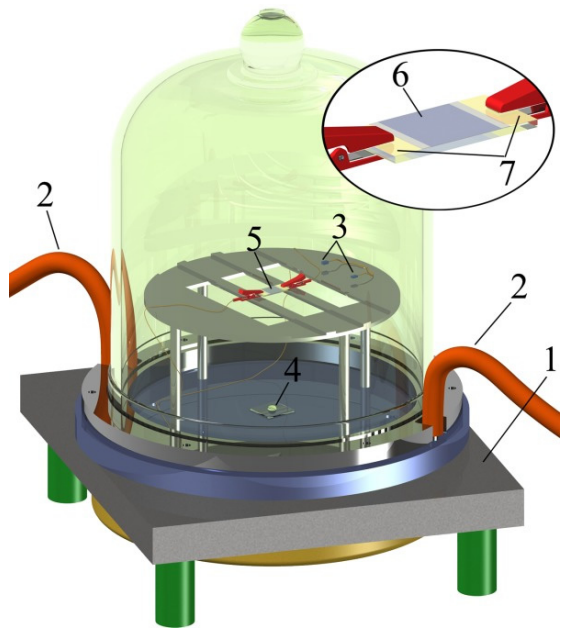

Figure 6. Chamber used for VPP of EDOT. The chamber is placed on a hot-plate (1), equipped with gas inlet valves connected to hoses (2), temperature and humidity sensors near the substrate (3). A source of EDOT vapors is a drop of EDOT on a glass slide at the bottom of the chamber (4). Polymerization occurs on the substrate above the EDOT drop (5). PEDOT film forms in the oxidant layer (6) and patterned ITO electrodes (7) enable to measure resistance *in situ* during film formation.

Pt-patterned substrates were used for preparing PEDOT films by LPDP. In general, the preparation method of PEDOT films by LPDP followed similar steps as the preparation of PEDOT films by VPP, but the monomer was deposited onto the substrates from solution. $Fe(Tos)_3$ oxidant films were prepared by spin-coating. Some of the films were subsequently dried at 80 °C, but undried films were also used for comparison. Polymerization was conducted in heptane solutions of EDOT at room temperature (21–22 °C) in a special cuvette designed for simultaneous measurements of resistance and optical transmittance. The obtained films were washed with methanol.

Electrochemical polymerization of PEDOT was carried out in a solution containing 0.1 M of EDOT and 0.1 M of *p*-toluenesulfonic acid, which were dissolved in deionized water-acetonitril mixture in a volume ratio of 1:1. The electropolymerized films were grown in a galvanostatic mode for 100 s using a current of 1 mA/cm^2 and as a counter-electrode 0.075 mm thick stainless steel foil (Goodfellow, AISI 316) was used. PEDOT composite film with the elastomer poly(1,6-hexanediol-co-citric acid) (PHC) used as one of the electrode materials in TENG was prepared according to the procedure described in the publication.[54]

3.3. Resistance measurements, atomic force microscopy, spectroscopic and grazing incidence X-ray diffraction characterization

Two-point resistance measurements were performed *in situ* during film growth and film aging. Temperature dependence of resistance was measured at low temperatures (10–150 K). AC of 20 Hz was used for *in situ* resistance measurements during VPP, but for other *in situ* resistance measurements DC was used. The used setup for two-point resistance measurements gave comparable R_s values to the values obtained by a four-point probe.

Four-point probe measurements were used to characterize the resistance of prepared PEDOT films. A four-point probe was equipped with gold-plated contacts spaced equally 2 mm apart in a linear configuration. The resistance of the films was generally measured in eight symmetrically positioned points on the film for films prepared on silicon-titanium mixed oxide coated glass substrates. The R_s values were calculated using accurate correction factors for specific measurement geometries by the method described in the literature.[63] Agilent 34410A multimeters were used for resistance measurements.

For PEDOT film thickness measurements, polymer films were scraped with a sharp needle, revealing the surface of the substrate. Atomic force microscope (AFM) (Veeco Dimension Edge) working in tapping mode was used for measuring the height difference between substrate surface and polymer surface. The thickness of the films was measured from at least three different locations averaging over several line scans for each location. AFM was also used for characterizing the surface morphology of the films.

The UV-Vis-NIR transmittance/absorbance spectra of washed PEDOT films were measured by JASCO V-570 spectrophotometer and Cary 5000 (Agilent Technologies) spectrophotometer. Transmittance of the PEDOT during LPDP was measured by Ocean Optics HR2000+ES spectrometer, using Ocean Optics LS-1 white light source. The measurement chamber was connected to the light source and spectrometer with optical fibers and collimator lenses with SMA 905 connector. Renishaw inVia micro-Raman spectrometer (spectral resolution 2 cm^{-1}) equipped with a continuous mode Ar^{+} gas laser (514.5 nm) was used for measuring Raman spectra. For XPS measurements a Gammadata Scienta SES-100 hemispherical energy analyzer and a non-monochromatised Mg K_{α} radiation source (a Thermo VG Scientific XR-4 X-ray gun) was used with overall resolution of approximately 0.6 eV. The XPS data were fitted with asymmetric line profiles (a Gaussian profile with an exponential tail on the high binding energy side), maintaining the same shape and width for all the six line components of the three line doublets, with the S 2p spin orbit splitting derived energy difference allowed to vary within 0.1 eV of the expected value of 1.15 eV. Grazing incidence X-ray diffraction (GIXRD) results were obtained by SmartLab (RigakuTM) diffractometer using 9 kW Cu rotating anode radiation source and a fixed 0.14° incidence angle.

3.4. Aging in different environments

Different gaseous environments (inert gas environments, oxygen, air, vacuum) were used for assessing the PEDOT film stability. Experiments at room temperature were performed in two-liter glass jars and in a stainless steel jar with a vacuum gauge for determining the effects of vacuum. The humidity of gaseous environments was regulated with saturated salt solutions in a humidity chamber prior to the aging experiments. A UV LED (110° viewing angle, 1 mW output power and peak wavelength at 370 nm) positioned 16 cm away from the film enabled to measure the effect of UV illumination on the stability of PEDOT. To avoid the influence of ambient lighting, the glass jars were covered with aluminum foil during the experiments. Thermal aging experiments were performed in an oven. Inert gas environment was created in a quartz tube with aluminum caps equipped with hoses. The data collection was started after the films were warmed up to the desired temperature to exclude the possible influence of temperature change on the resistance of the films.

4. RESULTS AND DISCUSSION

4.1. Preparation of PEDOT films by VPP (paper I)

The main objective of the first part of the study was to investigate the effect of preparation conditions on the properties (R_s, electrical conductivity and visible light transmittance) of VPP PEDOT films prepared in our polymerization chamber. However, significant additional insights into the polymerization process where gained during this investigation. Both increasing temperature at constant reaction time and reaction time at constant temperature resulted in similar outcomes in terms of transmittance, thickness, R_s and conductivity of the films (**Figure 7**). This offers evidence that to a large degree the effect of temperature and reaction time do not have a specific influence on the growth of PEDOT films and at higher temperatures growth proceeds in similar stages to growth at lower temperatures, only faster. Initially, film thickness increases slowly, but this is followed by a period of fast growth and finally the growth rate slows down again. Therefore, three different stages of film formation could be distinguished from these data. R_s reaches to a minimum value after the end of the second stage, but film thickness still slowly increases, transmittance decreases and conductivity decreases. Nonconductive polymer formation in the acidic environment may be responsible for this effect.[29] However, as the second part of this investigation demonstrates, washing out nonconductive material from PEDOT films seems to influence a well-formed PEDOT film surprisingly little, which casts doubt on this explanation. To some degree, PEDOT conductivity decay resulting from aging at elevated temperatures may also contribute to this.

Similar influence of increasing reaction time and temperature on conductivity implied that there should be a general relationship between the progress of film growth and the intrinsic parameters of PEDOT characterizing the specific growth stage. At constant initial oxidant concentration and oxidant film thickness, the resulting PEDOT film thickness should indicate the growth stage and the film should have properties characteristic to this stage. Indeed, plotting electrical conductivities as a function of thickness from several temperature and time series (previously shown series in **Figure 7** and additional series in similar conditions) reveals differences of PEDOT conductivities at different stages (**Figure 8**). At the first stage of growth, the PEDOT film conductivity is relatively high, exceeding considerably 1000 S/cm. The second stage is marked by absence of data points, because due to the rapid nature of film growth no PEDOT film from this stage was isolated. The third stage is marked by slow, but steady decline in film conductivity. The films exhibit the best properties for practical use as transparent conductors after the end of second stage of rapid growth. Although prior to the second stage the film conductivities are slightly higher, the films are very thin and could sometimes peel off from the substrate during washing with methanol.

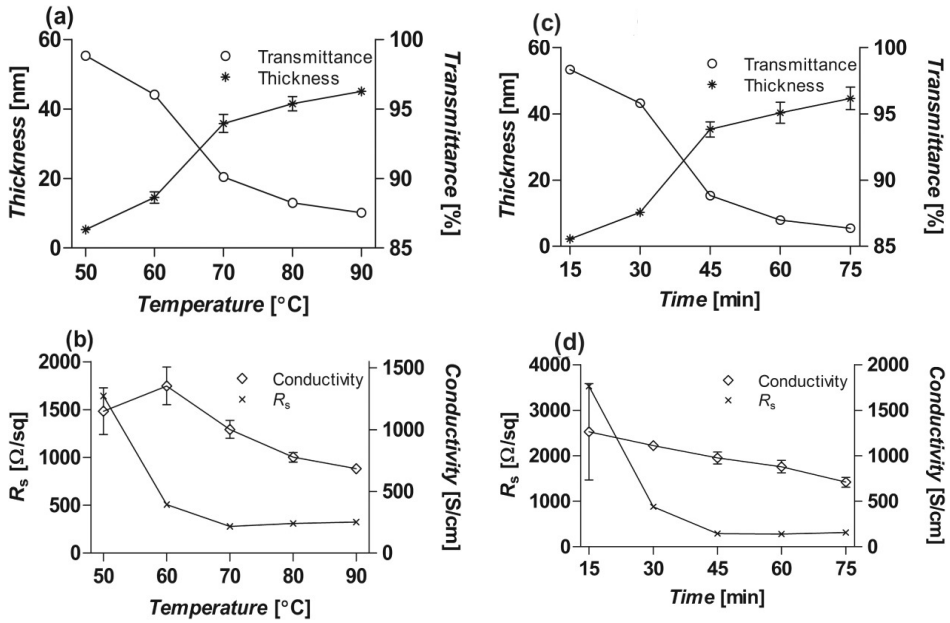

Figure 7. The effect of hot-plate temperature (at a reaction time of 30 min) on a) thickness and transmittance (at 550 nm), b) R_s and conductivity. The effect of polymerization time (at a hot-plate temperature of 60 °C) on c) thickness and transmittance (at 550 nm), d) R_s and conductivity.

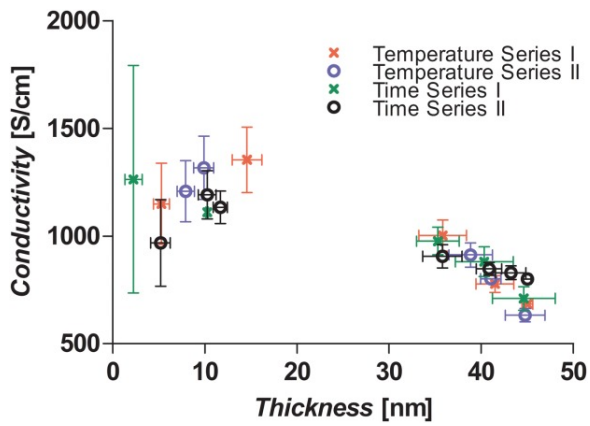

Figure 8. The dependence of VPP PEDOT film conductivity on PEDOT film thickness.

These results are mostly in agreement with the results obtained by Fabretto et al. and demonstrate that the preparation of PEDOT by base-inhibited version of VPP proceeds broadly in similar stages to VPP assisted by PEG-*ran*-PPG additive.[9] Both of these VPP processes are characterized by higher film conductivities obtained during initial slow polymerization, acceleration of polymer formation after the slow growth phase with a decrease of conductivity and finally again slow growth with a decline of conductivity. While Fabretto et al. distinguished two different polymerization stages before the rapid growth, according to the results reported in this study, only one stage precedes to the rapid growth. However, as measuring thickness of washed PEDOT films polymerized for a certain time in the reaction chamber is a much cruder method than the method used by Fabretto et al. (following mass increase *in situ* continuously during growth of a specific film), the differences between these stages could have remained unnoticed. In hope of obtaining better insight into the polymerization process, *in situ* resistance measurements were used to monitor the polymerization process.

In situ resistance measurements enabled to follow film growth at different relative humidities (RH) and oxidant solution concentrations (oxidant film thicknesses) (**Figure 9**). It has been determined that without enough water in the environment PEDOT does not form or has poor properties (e.g., a low conductivity), while too high RH causes crystallization of the oxidant and a patchy film formation.[12,25,43] RH did not reach to a sufficiently high value to have a detrimental effect on PEDOT film conductivity and other properties, but the lowest RH resulted in conductivities about three times lower than the highest RH. Resistance drops indicating percolation in the film started later for films prepared at lower RH values and lower oxidant solution concentrations. As expected, higher oxidant concentrations, which give higher $Fe(Tos)_3$ film thicknesses, result in thicker PEDOT films, but evidently some oxidant remains unreacted at lower RH values (**Figure 9d**).

During these experiments, a peculiar change in R_s value due to washing was noticed. This change ranged from –38% to +27% and lower (more negative) values of the R_s change were associated with lower RH values. This generated an idea that the progress of interconnected film formation could be monitored by using the change of resistance during washing. The change should depend on the ratio of polymer to oxidant and whether the percolation threshold is achieved or not. In **Figure 10**, which depicts resistance change due to washing, it is clearly seen that while the resistance of films polymerized for a short time drops several orders of magnitude during washing, the change is small and slightly positive for longer polymerized films. It could be deduced that for earlier stages of reaction progress, polymer-rich areas (presumably nodules according to AFM results) are separated to a large degree by nonconductive oxidant and reaction by-products, implying nodular growth. Washing the film removes nonconductive matter, PEDOT nodules become connected to each other and resistance drops dramatically. As PEDOT growth continues, finally interconnected PEDOT structure with an abundance of connective pathways

forms and nonconductive material has no significant influence on the resistance of the film. This interpretation was confirmed a few years after the publication of paper I, when the same trend in resistance change during washing was noticed by another research group, who varied the EDOT ratio to oxidant in a polymerizing solution.[21] The conductivities remained essentially the same in the washed PEDOT, but below a surprisingly low percolation threshold value (3% to 4.5% of PEDOT in oxidant matrix) washing caused a large decrease in resistance, but at high PEDOT content. Moreover, even a small increase in resistance due to washing was reported, what could be seen also as a result of our study.

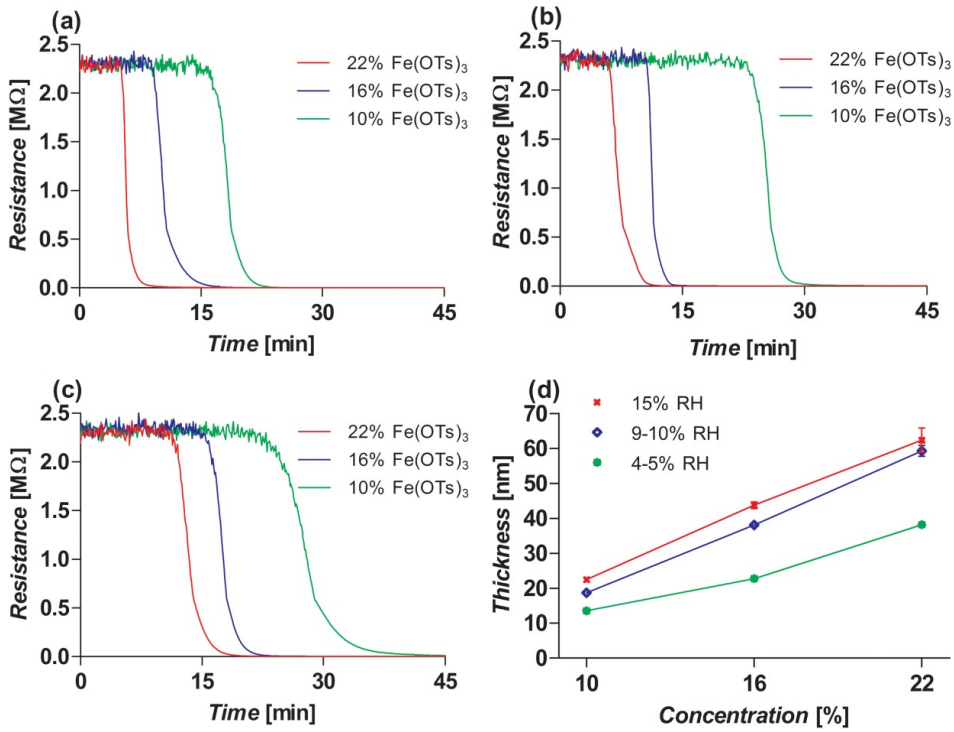

Figure 9. *In situ* measured R_s of PEDOT oxidant films prepared from 22%, 16% and 10% $Fe(Tos)_3$ solutions at a) 15% RH, b) 9–10% RH and c) 4–5% RH in the polymerization chamber. d) The influence of $Fe(Tos)_3$ solution concentration on the PEDOT film final thickness for films polymerized at 4–5% RH, 9–10% RH, and 15% RH. For all the experiments, the hot-plate temperature was 60 °C and total polymerization time 60 minutes.

The exact basis of conductivity variation between films at different polymerization stages remains inconclusive. No significant differences between the Raman spectra of polymer films are detectable. The inter-chain stacking is similar for all samples, although there was intensity variation implying different degree

of order in different polymer films normal to the plane of substrate (**Figure 11**). The lowest intensity was recorded for the film polymerized at low RH, which may explain low conductivity. However, there was no clear straightforward trend in the GIXRD results. The relation between the order in chain alignment and conductivity in base-inhibited VPP PEDOT is doubtful.[21] Slight increase in surface roughness after the period of quick growth may also be related to the lower conductivities. Generally, as conduction in PEDOT may be sensitive to a variety of parameters and the detailed conduction mechanism of PEDOT is still under intense debate, it is difficult to gain a clear view of the exact reasons of conductivity variation.

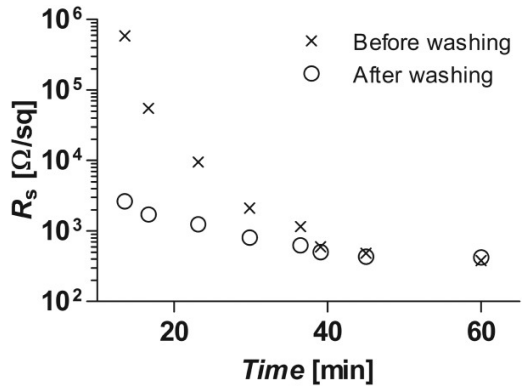

Figure 10. PEDOT-oxidant film R_s before washing and the R_s of the same film after washing out nonconductive material. The films were prepared at 14–18% RH and at a hot-plate temperature of 60 °C.

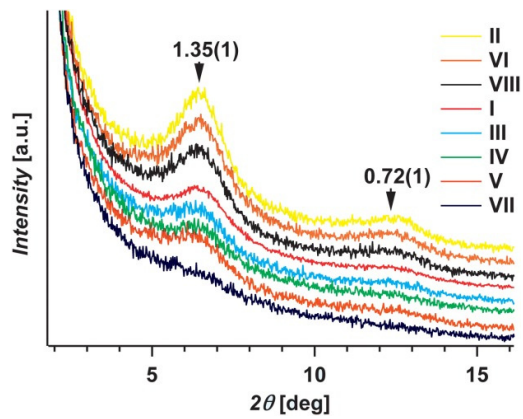

Figure 11. GIXRD patterns for different PEDOT films polymerized for 15 min (I), 45 min (II), 75 min (III) at a hot-plate temperature of 60 °C, for 30 min at a hot-plate temperature of 50 °C (IV), 70 °C (V), 90 °C (VI), for 60 min at a hot-plate temperature of 60 °C at low RH of 4–5% (VII) and high RH of 15% (VIII).

In conclusion, base-inhibited VPP enables to prepare PEDOT films with relatively high conductivity compared to most formulations of PEDOT:PSS and electropolymerized PEDOT, but still lacks the high conductivity and transparency of commercial ITO or best PEDOT films. The minimum value of R_s was ~280 Ω/sq, still more than an order of magnitude higher than corresponding value for commercial ITO and the best conductivity ~1350 S/cm, which is ~1/3 of commercial ITO conductivity. The choice of proper preparation conditions is crucial for obtaining high quality PEDOT films.

4.2. Preparation of PEDOT films by LPDP (paper II)

The aim of the second part of the study was to prepare PEDOT films by a relatively recently proposed EDOT preparation method LPDP and compare the method to a more well-established VPP. In principle, as the source of EDOT monomer is a solution in VPP, it is easier to control the concentration of EDOT and guarantee homogeneous distribution of the monomer. For gaining a thorough overview of the LPDP process, *in situ* resistance measurements were combined with *in situ* transmittance measurements. Previously dried and undried oxidant films were used for comparison.

In **Figure 12** simultaneous measurements of transmittance and resistance are depicted at different EDOT concentrations for polymerizing undried $Fe(Tos)_3$-PEDOT films and in **Figure 13** analogous measurements for polymerizing dried $Fe(Tos)_3$-PEDOT films. With higher EDOT concentrations, polymerization proceeded faster. It is interesting to note that compared to VPP, much higher EDOT concentrations in the polymerization chamber are necessary, probably due to the EDOT propensity to remain in the nonpolar solvent phase. For dried films the polymerization times were significantly longer and higher EDOT concentrations were required to achieve similar polymerization rates to undried films. Generally, according to transmittance change three stages of growth occur at lower EDOT concentrations. Like for VPP of EDOT, an initial stage of slow growth is followed by a period of quicker growth prior to a decrease of growth rate at the end of reaction, when oxidant supply is low. At higher EDOT concentrations the initial stage of slow growth was not detectable, likely due to a general overall large reaction rate increase compared to reactions at lower concentrations. Some curves depict additional variation in growth rate, but generally the tree-stage description fits quite well for lower concentrations and two-stage description for higher concentrations. For several films a small drop in transmittance (~0.5%) was evident before the second stage of quick growth. This implies percolation, which must occur according to the low transmittance value at a very low amount of PEDOT, implying film formation at the interface, not homogeneously inside the oxidant film.

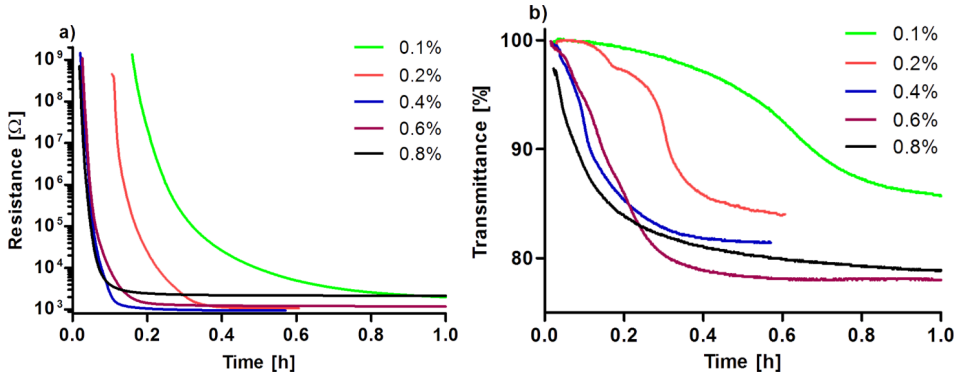

Figure 12. a) Resistance and b) transmittance (at 700 nm) of polymerizing undried $Fe(Tos)_3$-PEDOT films in solutions containing 0.1%–0.8% EDOT (v/v).

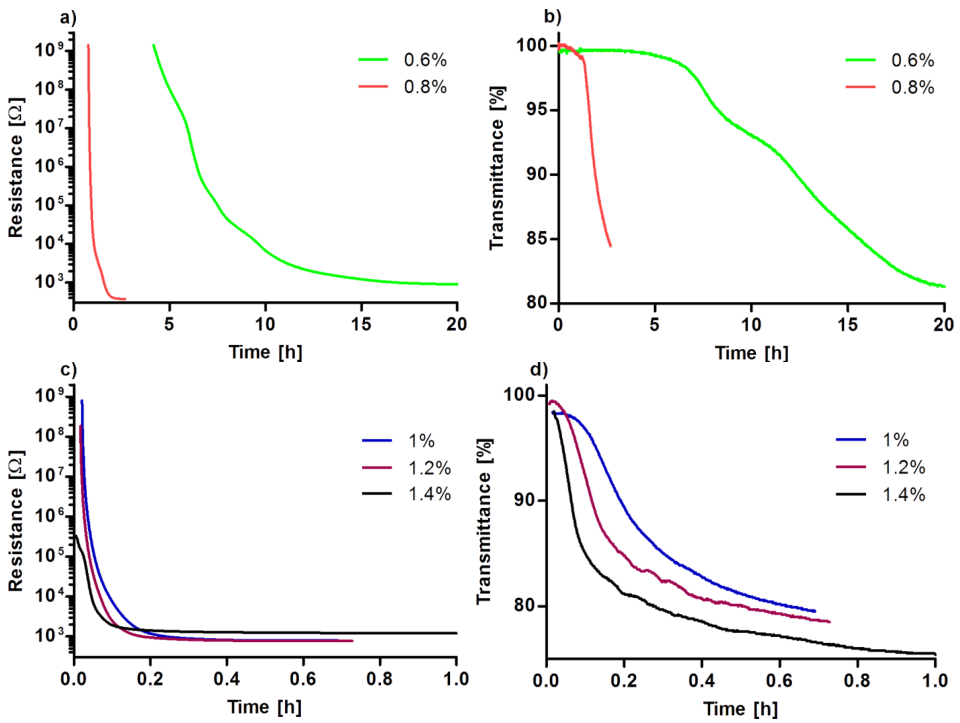

Figure 13. a) Resistance and b) transmittance (at 700 nm) of polymerizing dried $Fe(Tos)_3$-PEDOT films in 0.6% and 0.8% (v/v) EDOT solutions. c) Resistance and d) transmittance (at 700 nm) of polymerizing dried PEDOT films in 1%–1.4% (v/v) EDOT solutions. As the polymerization times were extremely long for dried films in 0.6% and 0.8% EDOT solution, these graphs are depicted separately from others for clarity.

With longer polymerization times, resistance of the films achieved a plateau value, while the transmittance slowly, but continuously decreased. This shows

that similarly to VPP, the quality of the films decreases in the later polymerization stages. UV-Vis-NIR spectra (**Figure 14**) revealed that with longer polymerization period shorter oligomers were likely to form. It is evidenced by an increase in UV absorbance[44] and decrease in the band associated with bipolarons[64] for extremely long polymerization time (40 h).

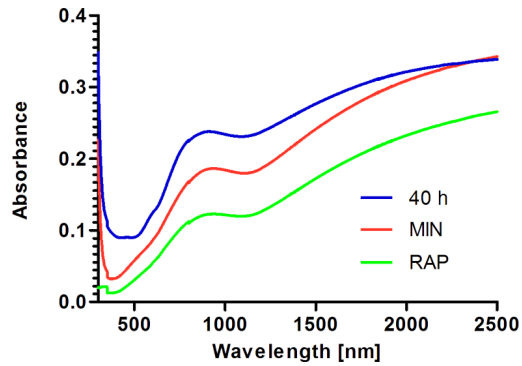

Figure 14. UV–Vis-NIR absorbance spectra in the range of 300 to 2500 nm for films, which polymerization was terminated at rapid growth (RAP), at resistance minimum (MIN) and after 40 h of growth (40 h).

Both dried and undried oxidant films gave generally higher conductivities at lower EDOT concentrations (**Figure 15**). Although PEDOT films prepared from dried $Fe(Tos)_3$ have higher conductivities than the ones from undried oxidant films, these values are still much lower than the results for VPP PEDOT. Drying of the oxidant layer has been already earlier reported to have positive effect on LPDP PEDOT R_s.[38]

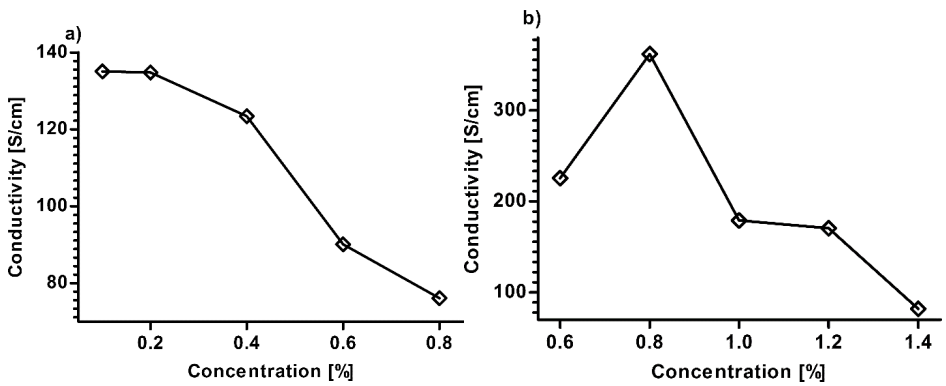

Figure 15. a) Electrical conductivity of PEDOT films prepared from undried $Fe(Tos)_3$ films and b) electrical conductivity of PEDOT films prepared from dried $Fe(Tos)_3$ films.

PEDOT films prepared by LPDP had high surface roughness. Root mean squared (RMS) roughness values were in the range of 6.3 nm to 17.1 nm for the previously described PEDOT film series from dried oxidant films and in the range of 10.5 nm to 30.7 nm for the PEDOT series from undried oxidant films. These values are significantly higher than the values for VPP PEDOT films (RMS roughness around few nm). Typical surface morphologies showed oxidant crystal formation and even structures showing possible phase separation. **Figure 16** depicts the morphologies of PEDOT films prepared from the undried $Fe(Tos)_3$ as examples of PEDOT films with rough surfaces.

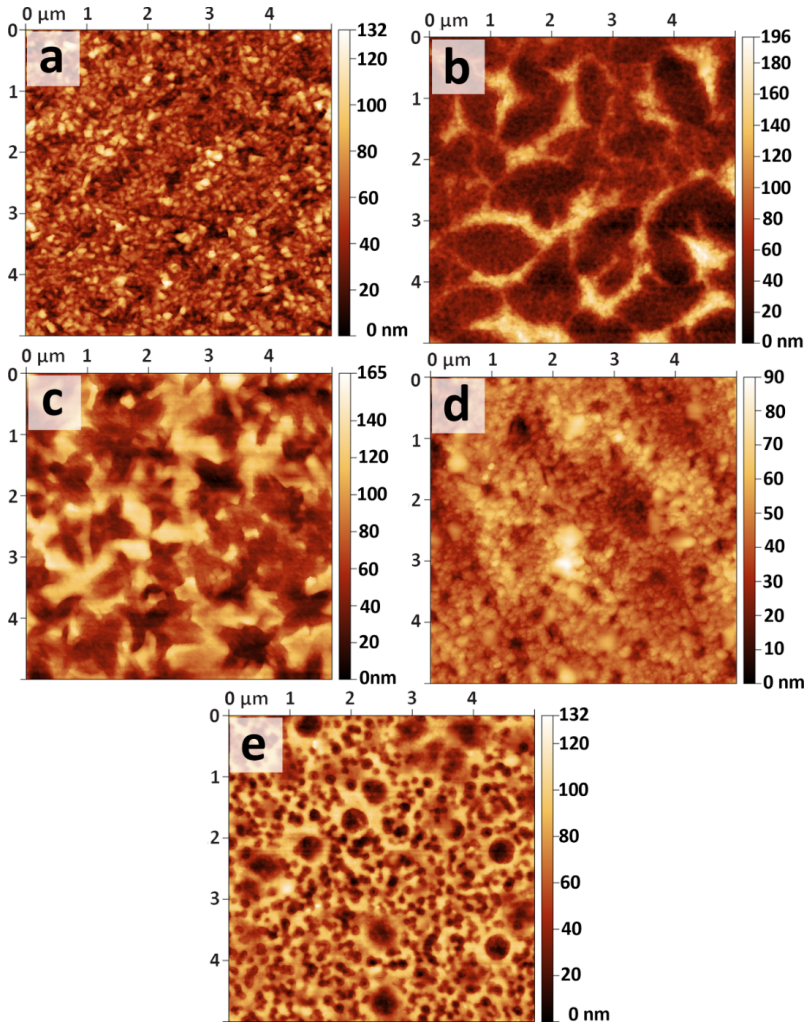

Figure 16. AFM images of the PEDOT films prepared from undried oxidant films (RMS roughness indicated in parenthesis) in a) 0.1% (18.0 nm); b) 0.2% (30.7 nm); c) 0.4% (27.6 nm); d) 0.6% (10.5 nm) and e) 0.8% (21.3 nm) EDOT solutions.

Although LPDP allows better control over EDOT distribution, controlling surface morphology is difficult and this method needs further development to be competitive with VPP. Relatively low conductivities and rough uneven surface with holes almost reaching down to the substrate indicate that there is still a need for large improvement of film properties. However, as the method is relatively novel, there are only a few reports in the literature and likely the full potential of the method has not been discovered. Recently reported oxidative post-treatment is one of the options, which improves the conductivity of LPDP films significantly.[39]

4.3. Stability of PEDOT films prepared by VPP (paper III)

The aim of paper III was to investigate the stability of PEDOT film conductance in different environments and to find the conditions most suitable regarding polymer stability. For determining PEDOT stability, VPP PEDOT as a relatively highly conductive material was chosen. From a practical point of view, stability is frequently the factor that limits the actual usefulness of ICPs. For this investigation, different gaseous environments were used, both at room temperature and at elevated temperatures. Oxygen and water vapor are usually thought to be the main factors behind this degradation, but a systematic study of different parameters influencing the conducting system is necessary. Although there are some reports about the stability of VPP PEDOT films, these reports have not been focused on systematic study of various working conditions.

The influence of increasing temperature unsurprisingly accelerates the degradation of film conductance (**Figure 17**). However, surprisingly degradation of conductance at 140 °C was as fast in the argon environment than in the air. This degradation of conductance was not well explained over the measured range by previously established models like diffusion-controlled aging or shrinking in conductive grains compared to widening of insulating barriers described in polypyrrole[65] or PEDOT:PSS[7], also pseudo-exponential decay previously attributed to PEDOT:Tos did not describe the situation.[66] To determine the specific model suitable for describing the aging mechanism requires additional in-depth study, which is not the purpose of this work.

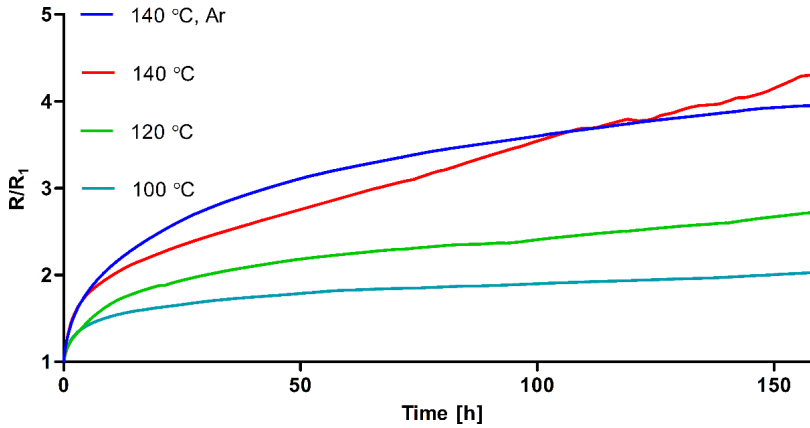

Figure 17. PEDOT film resistance stability (depicted as resistance normalized to initial value) at different temperatures (100 °C, 120 °C and 140 °C) in air and under argon flow at 140 °C (140 °C, Ar).

Resistance increases (**Figure 18**) at room temperature conditions were considerably smaller than resistance increases at elevated temperatures. As for accelerated aging experiments, previously described simple models did not explain the degradation properly in the duration of the experiment. Generally, humidity and UV light increased the degradation of film conductance. Humidity influenced the films detrimentally at least for a few first days of the experiment, later the degradation rates were comparable in dry and humid dark environments. Interestingly, vacuum had similar effect of increasing the resistance to water vapor. It is possible, that there is some complex relationship between the conductivity and transport of small molecules between films and the environment. UV illumination caused significant increase of resistance in both dry nitrogen and oxygen. Unexpectedly, the oxygen environment did not accelerate the aging at all compared to nitrogen environment, although light-induced degradation in PEDOT has been associated with a mechanism involving oxidation by singlet oxygen.[67] However, it is not possible to exclude the influence of oxygen totally, as the films were prepared in ambient conditions and were not subjected to long vacuum treatment before the aging experiment. PEDOT conductivity was the most stable in dark and dry environments, but even in these environments the resistance increased almost up to 0.5% per day.

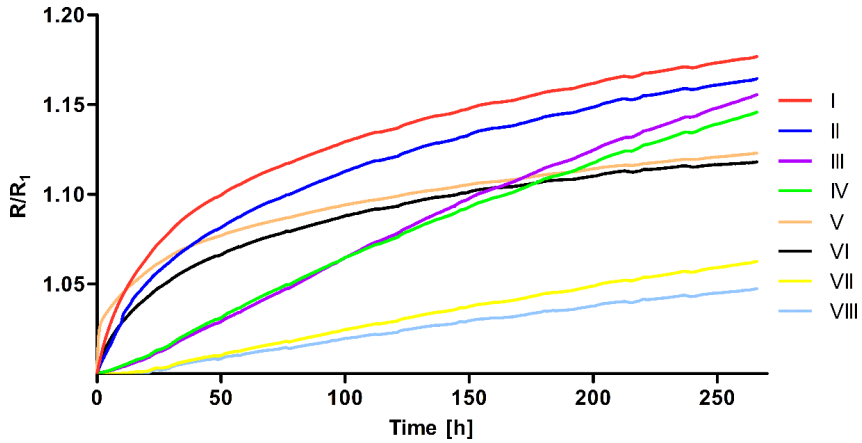

Figure 18. The influence of aging in different environments on PEDOT film resistance (normalized to initial value). The different environments are following: I – 20 mbar vacuum, II – N_2 with 59% RH, III – UV illumination in dry O_2, IV – UV illumination in dry N_2, V – UV illumination in humid O_2 with 59% RH, VI – O_2 with 58% RH, VII – dry O_2, VIII – dry N_2.

The influence of temperature on the resistance of a thermally aged film and freshly prepared film is depicted in **Figure 19**. According to **equation 1** the resistance of the aged film could be described by 3-D variable-range hopping (**Figure 19b**), while the freshly prepared film seems to be in the critical regime of IMT[5] (**Figure 19c**). Freshly prepared samples with low resistance are near to IMT as evidenced by α values close to zero, while α values (0.2–0.3) for thermally aged samples correspond better to 2-D or 3-D variable-range hopping. The critical regime depends on the disorder in the polymer films.[5] This implies that thermal aging causes IMT by increasing some kind of disorder in the polymer film, although it does not reveal the nature of this disorder.

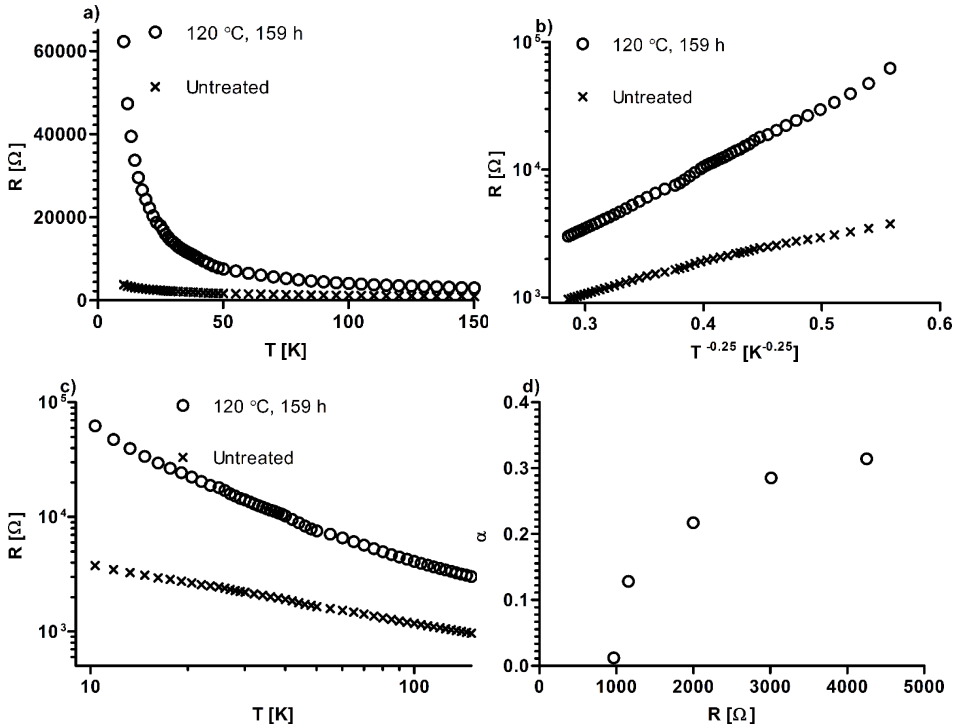

Figure 19. Temperature dependence of resistance for a freshly prepared PEDOT film and a film aged at 120 °C for 159 h as a) R versus T; b) R versus $T^{-0.25}$; c) R versus T on a log-log scale. d) α values for PEDOT films depending on the resistance of the films at 150 K.

While in the Raman spectra of aged films there were no significant differences, UV-Vis-NIR spectra were different for the freshly prepared and aged films (**Figure 20**). An absorbance maximum appears at ~940 nm and absorbance increases also at ~600 nm, the latter change being especially visible for the film heated in argon (**Figure 20c**), but at higher wavelengths absorbance decreases with aging. Absorbance maximum at ~600 nm is assigned to neutral PEDOT, ~800 nm to polaron states and the broad absorbance band ~1800 nm to bipolaron states.[64] During electrochemical reduction, similar spectral changes to the changes depicted in **Figure 20** occur.[68] Therefore, these changes may be associated with a decrease in charge carrier density. However, charge carrier redistribution between different states due to structural changes is also a possibility.[69] These spectral changes show that charge carrier properties of PEDOT have been changed. In some cases, these spectral features could still have surprisingly little influence on PEDOT conductivity.[21] However, it is clear that these changes decrease slightly the transparency of the films.

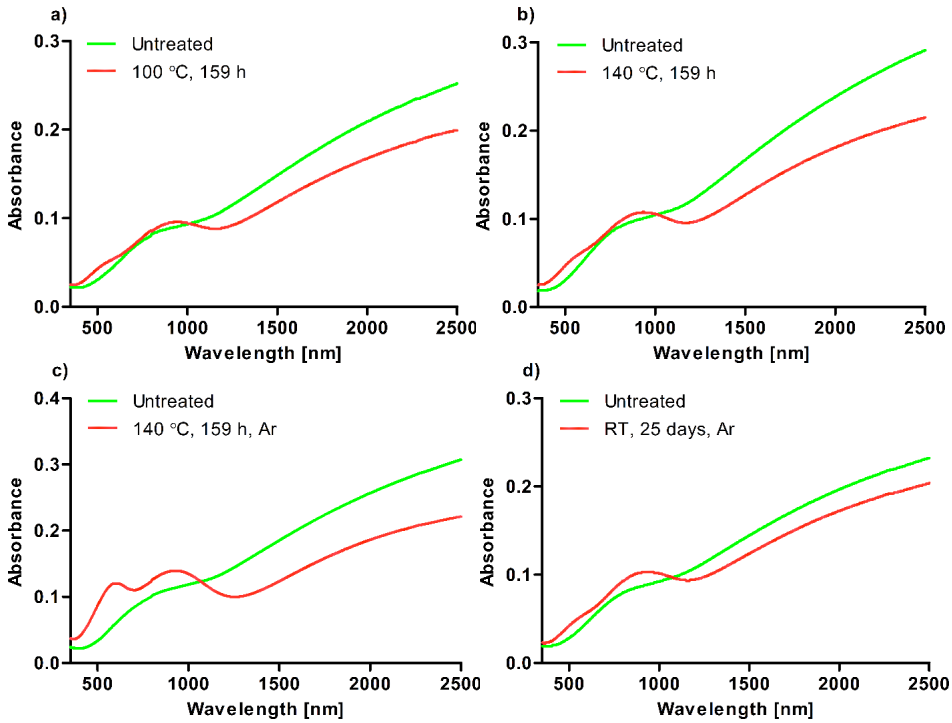

Figure 20. UV-Vis-NIR absorbance spectra (350–2500 nm) of freshly prepared PEDOT films and the same films aged for a) 159 h at 100 °C in air; b) 159 h at 140 °C in air; c) 159 h at 140 °C in argon flow; d) 25 days at room temperature in argon environment.

XPS results showed that there is some evidence of chemical changes occurring during thermal aging in the surface layer of the film. Generally, three different kinds of sulfur atoms were detectable with S($2p_{3/2}$) lines at 163.1 eV (thiophene S), 166.3 eV (*p*-toluenesulfonate S) and 167.7 eV (oxidized S). While the freshly prepared films and the films aged at room temperature in inert gas (in dark or under UV light) had thiophene and *p*-toluenesulfonate lines and almost no additional oxidized S, thermally aged films had a high proportion of oxidized S. However, as no significant changes take place according to Raman spectroscopy or GIXRD results and XPS is surface sensitive, these may be related to surface processes, which have no significant influence on film properties.

In conclusion, it is possible to slow down the degradation of VPP PEDOT conductance by using the films in dark and dry environments. However, even this will not enable to avoid completely the decrease of PEDOT film conductance. For more sensitive applications to conductance stability, this may be problematic.

4.4. PEDOT electrode as a replacement for ITO electrode in TENGs (paper IV)

Finally, PEDOT electrodes were tested as a working electrode and a contact surface for a replacement of ITO in a specific potential application, TENG. The fabrication of TENGs is a rapidly developing research area, for which novel materials are useful. To our best knowledge, PEDOT has not been used as a contact surface in this kind of device. This application does not require especially high conductivity, which alleviates the potential stability problems of PEDOT.

In **Figure 21**, current densities, power densities and voltages from TENGs containing different PEDOT-based electrodes/contact surfaces (VPP PEDOT, electropolymerized PEDOT and PEDOT/PHC elastomeric composite) in comparison with ITO are depicted. The highest peak current density (0.45 mA/m^2) and peak power density (95 W/m^2) were generated by VPP PEDOT electrode. In conjunction with PDMS used in specific TENGs, PEDOT is a better contact surface than commercial ITO, because it generates ~3 higher power density. VPP PEDOT generates also the highest voltage. The performance for other PEDOT-based electrodes is worse compared to ITO. All the PEDOT electrodes exhibited continuous output without stability issues for more than 1000 cycles.

The observed differences between electrode performances were not related to R_s values. While electropolymerized PEDOT had much higher RMS roughness (34.09 nm) than VPP PEDOT (1.88 nm) and even PEDOT/PHC had higher RMS roughness (7.35 nm), the performance was much better for VPP PEDOT. Higher contact surface area should improve the TENG performance,[70] therefore, the results are somewhat counterintuitive. However, as PDMS contact surface was smooth, effective surface area may have been larger for the smooth PEDOT. Also, the chemical differences between surfaces may be important in determining the performance of the device. Differences in work function, heterolytic bond breaking, mechanical properties of the material and concentration of mobile ions (*p*-toluenesulfonate) on the surface may all be important for TENG performance.

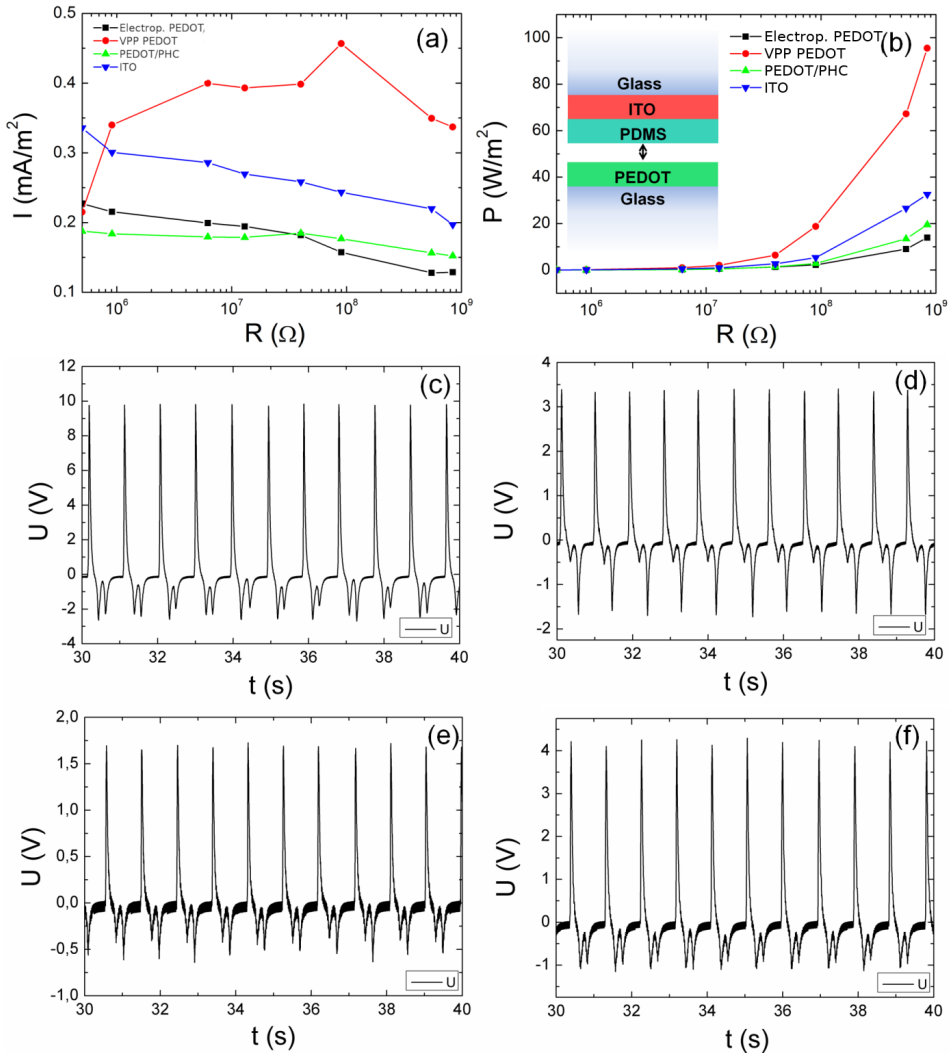

Figure 21. Measured TENG performance with different contact electrodes. a) Measured current versus load resistance, b) calculated power density versus load resistance (inset shows schematic illustration of layered structure of TENG), c) measured voltage for VPP PEDOT, d) PEDOT/PHC, e) electropolymerized PEDOT and f) ITO contact electrodes by contacting with PDMS at the circuit resistance of 90 MΩ.

CONCLUSIONS

VPP and LPDP are two different methods of oxidative polymerization, which were used for preparing ICP PEDOT films in this thesis. During VPP PEDOT, thin films with relatively high conductance and transparency (90% transmittance at 550 nm at a R_s below 300 Ω/sq) were prepared. The best conductivity values exceeded 1300 S/cm. The influence of temperature, growth time, concentration of oxidant solution and relative humidity on the optical and electrical properties of the films was investigated and suitable conditions for film preparation were determined. Three different stages of growth, which resulted in films with different properties, were detected. Washing of the as-prepared PEDOT/oxidant films in an early growth stage caused a large decrease in resistances, implying nodular growth of PEDOT during film formation.

Compared to VPP, the polymer films prepared by LPDP had lower conductivities and a defective surface microstructure. *In situ* transmittance measurements were combined with simultaneous *in situ* resistance measurements for a closer overview of polymerization process, revealing a three-stage polymerization process similar to the polymerization during VPP.

In situ resistance measurements were used to assess the stability of VPP PEDOT films both at room temperature and elevated temperatures in different gaseous environments. PEDOT had relatively high stability in dry and dark environments at room temperature, although even in these cases a slight linear increase of resistance (~4–5% per 10 days) occurred. UV illumination, water vapor and, surprisingly, vacuum conditions caused significant additional resistance increase at room temperature. Aging was accelerated by raising the temperature up to 140 °C and at elevated temperatures both inert gas environment and air resulted in comparable aging. Characteristic changes in UV-Vis-NIR absorption spectra for aged films indicates changes in polaron and bipolaron states in the material. Low-temperature resistance measurements revealed that while freshly prepared PEDOT films display conductance properties characteristic to the critical regime at metal-insulator transition, thermally aged samples correspond better to a 2-D or 3-D variable range hopping model in insulating regime.

PEDOT films were used as both a contact surface and as an electrode in TENGs, which convert mechanical energy to electrical energy. VPP PEDOT was superior compared to ITO, generating approximately three times higher power density. VPP PEDOT-containing device exhibited stable output for more than 1000 cycles, demonstrating the suitability of PEDOT for this application.

REFERENCES

(1) Shirakawa, H.; Louis, E. J.; MacDiarmid, A. G.; Chiang, C. K.; Heeger, A. J. Synthesis of Electrically Conducting Organic Polymers: Halogen Derivatives of Polyacetylene, (CH)X. *J. Chem. Soc. Chem. Commun.* **1977**, *0* (16), 578–580.

(2) Chiang, C. K.; Fincher, C. R.; Park, Y. W.; Heeger, A. J.; Shirakawa, H.; Louis, E. J.; Gau, S. C.; MacDiarmid, A. G. Electrical Conductivity in Doped Polyacetylene. *Phys. Rev. Lett.* **1977**, *39* (17), 1098–1101.

(3) Elschner, A.; Kirchmeyer, S.; Lovenich, W.; Merker, U.; Reuter, K. *PEDOT: Principles and Applications of an Intrinsically Conductive Polymer*; CRC Press, 2010.

(4) Blythe, A. R.; Blythe, T.; Bloor, D. *Electrical Properties of Polymers*; Cambridge University Press, 2005.

(5) Heeger, A. J. Disorder-Induced Metal–Insulator Transition in Conducting Polymers. *J. Supercond.* **2001**, *14* (2), 261–268.

(6) Padmalekha, K. G.; Admassie, S. Electrochromic, Magnetotransport and AC Transport Properties of Vapor Phase Polymerized PEDOT (VPP PEDOT). *Synth. Met.* **2009**, *159* (17), 1885–1889.

(7) Vitoratos, E.; Sakkopoulos, S.; Dalas, E.; Paliatsas, N.; Karageorgopoulos, D.; Petraki, F.; Kennou, S.; Choulis, S. A. Thermal Degradation Mechanisms of PEDOT:PSS. *Org. Electron.* **2009**, *10* (1), 61–66.

(8) Groenendaal, L.; Jonas, F.; Freitag, D.; Pielartzik, H.; Reynolds, J. R. Poly(3,4-Ethylenedioxythiophene) and Its Derivatives: Past, Present, and Future. *Adv. Mater.* **2000**, *12* (7), 481–494.

(9) Fabretto, M.; Müller, M.; Hall, C.; Murphy, P.; Short, R. D.; Griesser, H. J. In-situ QCM-D Analysis Reveals Four Distinct Stages during Vapour Phase Polymerisation of PEDOT Thin Films. *Polymer* **2010**, *51* (8), 1737–1743.

(10) Crispin, X.; Marciniak, S.; Osikowicz, W.; Zotti, G.; Gon, A. W. D. van der; Louwet, F.; Fahlman, M.; Groenendaal, L.; Schryver, F. D.; Salaneck, W. R. Conductivity, Morphology, Interfacial Chemistry, and Stability of Poly(3,4-Ethylene Dioxythiophene)–Poly(Styrene Sulfonate): A Photoelectron Spectroscopy Study. *J. Polym. Sci. Part B Polym. Phys.* **2003**, *41* (21), 2561–2583.

(11) Metsik, J.; Timusk, M.; Käämbre, T.; Mändar, H.; Umalas, M.; Kuus, A.; Puust, L.; Utt, K.; Sildos, I.; Mäeorg, U. Stability of Poly(3,4-Ethylenedioxythiophene) Thin Films Prepared by Vapor Phase Polymerization. *Polym. Degrad. Stab.* **2016**, *126*, 170–178.

(12) Fabretto, M.; Zuber, K.; Hall, C.; Murphy, P.; J. Griesser, H. The Role of Water in the Synthesis and Performance of Vapour Phase Polymerised PEDOT Electrochromic Devices. *J. Mater. Chem.* **2009**, *19* (42), 7871–7878.

(13) Rudd, S.; Franco-Gonzalez, J. F.; Singh, S. K.; Khan, Z. U.; Crispin, X.; Andreasen, J. W.; Zozoulenko, I.; Evans, D. Charge Transport and Structure in Semimetallic Polymers. *J. Polym. Sci. Part B Polym. Phys.* **2018**, *56* (1), 97–104.

(14) Lee, S.; Paine, D. C.; Gleason, K. K. Heavily Doped Poly(3,4-Ethylenedioxythiophene) Thin Films with High Carrier Mobility Deposited Using Oxidative CVD: Conductivity Stability and Carrier Transport. *Adv. Funct. Mater.* **2014**, *24* (45), 7187–7196.

(15) Massonnet, N.; Carella, A.; Geyer, A. de; Faure-Vincent, J.; Simonato, J.-P. Metallic Behaviour of Acid Doped Highly Conductive Polymers. *Chem. Sci.* **2014**, *6* (1), 412–417.

(16) Gueye, M. N.; Carella, A.; Massonnet, N.; Yvenou, E.; Brenet, S.; Faure-Vincent, J.; Pouget, S.; Rieutord, F.; Okuno, H.; Benayad, A.; et al. Structure and Dopant Engineering in PEDOT Thin Films: Practical Tools for a Dramatic Conductivity Enhancement. *Chem. Mater.* **2016**, *28* (10), 3462–3468.
(17) Farka, D.; Coskun, H.; Gasiorowski, J.; Cobet, C.; Hingerl, K.; Uiberlacker, L. M.; Hild, S.; Greunz, T.; Stifter, D.; Sariciftci, N. S.; et al. Anderson-Localization and the Mott–Ioffe–Regel Limit in Glassy-Metallic PEDOT. *Adv. Electron. Mater.* **2017**, *3* (7), 1700050.
(18) Bubnova, O.; Khan, Z. U.; Wang, H.; Braun, S.; Evans, D. R.; Fabretto, M.; Hojati-Talemi, P.; Dagnelund, D.; Arlin, J.-B.; Geerts, Y. H.; et al. Semi-Metallic Polymers. *Nat. Mater.* **2014**, *13* (2), 190–194.
(19) Cho, B.; Park, K. S.; Baek, J.; Oh, H. S.; Koo Lee, Y.-E.; Sung, M. M. Single-Crystal Poly(3,4-Ethylenedioxythiophene) Nanowires with Ultrahigh Conductivity. *Nano Lett.* **2014**, *14* (6), 3321–3327.
(20) Fabretto, M. V.; Evans, D. R.; Mueller, M.; Zuber, K.; Hojati-Talemi, P.; Short, R. D.; Wallace, G. G.; Murphy, P. J. Polymeric Material with Metal-Like Conductivity for Next Generation Organic Electronic Devices. *Chem. Mater.* **2012**, *24* (20), 3998–4003.
(21) Mayevsky, D.; Gann, E.; Garvey, C. J.; McNeill, C. R.; Winther-Jensen, B. Decoupling Order and Conductivity in Doped Conducting Polymers. *Phys. Chem. Chem. Phys.* **2016**, *18* (28), 19397–19404.
(22) Worfolk, B. J.; Andrews, S. C.; Park, S.; Reinspach, J.; Liu, N.; Toney, M. F.; Mannsfeld, S. C. B.; Bao, Z. Ultrahigh Electrical Conductivity in Solution-Sheared Polymeric Transparent Films. *Proc. Natl. Acad. Sci. U. S. A.* **2015**, *112* (46), 14138–14143.
(23) Lock, J. P.; Im, S. G.; Gleason, K. K. Oxidative Chemical Vapor Deposition of Electrically Conducting Poly(3,4-Ethylenedioxythiophene) Films. *Macromolecules* **2006**, *39* (16), 5326–5329.
(24) Castagnola, V.; Bayon, C.; Descamps, E.; Bergaud, C. Morphology and Conductivity of PEDOT Layers Produced by Different Electrochemical Routes. *Synth. Met.* **2014**, *189*, 7–16.
(25) Zuber, K.; Fabretto, M.; Hall, C.; Murphy, P. Improved PEDOT Conductivity via Suppression of Crystallite Formation in Fe(III) Tosylate During Vapor Phase Polymerization. *Macromol. Rapid Commun.* **2008**, *29* (18), 1503–1508.
(26) Badre, C.; Marquant, L.; Alsayed, A. M.; Hough, L. A. Highly Conductive Poly(3,4-Ethylenedioxythiophene):Poly (Styrenesulfonate) Films Using 1-Ethyl-3-Methylimidazolium Tetracyanoborate Ionic Liquid. *Adv. Funct. Mater.* **2012**, *22* (13), 2723–2727.
(27) Xia, Y.; Sun, K.; Ouyang, J. Solution-Processed Metallic Conducting Polymer Films as Transparent Electrode of Optoelectronic Devices. *Adv. Mater.* **2012**, *24* (18), 2436–2440.
(28) Winther-Jensen, B.; Breiby, D. W.; West, K. Base Inhibited Oxidative Polymerization of 3,4-Ethylenedioxythiophene with Iron(III)Tosylate. *Synth. Met.* **2005**, *152* (1), 1–4.
(29) Winther-Jensen, B.; West, K. Vapor-Phase Polymerization of 3,4-Ethylenedioxythiophene: A Route to Highly Conducting Polymer Surface Layers. *Macromolecules* **2004**, *37* (12), 4538–4543.

(30) Ha, Y.-H.; Nikolov, N.; Pollack, S. K.; Mastrangelo, J.; Martin, B. D.; Shashidhar, R. Towards a Transparent, Highly Conductive Poly(3,4-Ethylenedioxythiophene). *Adv. Funct. Mater.* **2004**, *14* (6), 615–622.
(31) Brooke, R.; Cottis, P.; Talemi, P.; Fabretto, M.; Murphy, P.; Evans, D. Recent Advances in the Synthesis of Conducting Polymers from the Vapour Phase. *Prog. Mater. Sci.* **2017**, *86*, 127–146.
(32) Truong, T. L.; Luong, N. D.; Nam, J.-D.; Lee, Y.; Choi, H. R.; Koo, J. C.; Nguyen, H. N. Poly(3,4-Ethylenedioxythiophene) Vapor-Phase Polymerization on Glass Substrate for Enhanced Surface Smoothness and Electrical Conductivity. *Macromol. Res.* **2007**, *15* (5), 465–468.
(33) Evans, D.; Fabretto, M.; Mueller, M.; Zuber, K.; Short, R.; Murphy, P. Structure-Directed Growth of High Conductivity PEDOT from Liquid-like Oxidant Layers during Vacuum Vapor Phase Polymerization. *J. Mater. Chem.* **2012**, *22* (30), 14889–14895.
(34) Fabretto, M.; Müller, M.; Zuber, K.; Murphy, P. Influence of PEG-ran-PPG Surfactant on Vapour Phase Polymerised PEDOT Thin Films. *Macromol. Rapid Commun.* **2009**, *30* (21), 1846–1851.
(35) 1H-Imidazole https://webbook.nist.gov/cgi/cbook.cgi?Name=imidazole&Units= SI (accessed Jun 5, 2018).
(36) de Jong, M. P.; van IJzendoorn, L. J.; de Voigt, M. J. A. Stability of the Interface between Indium-Tin-Oxide and Poly(3,4-Ethylenedioxythiophene)/ Poly(Styrenesulfonate) in Polymer Light-Emitting Diodes. *Appl. Phys. Lett.* **2000**, *77* (14), 2255–2257.
(37) Li, J.; Zhang, M.; Liu, J.; Ma, Y. Effect of Attached Peroxyacid on Liquid Phase Depositional Polymerization of EDOT over PI Film with Adsorbed Ferric Chloride. *Synth. Met.* **2014**, *198*, 161–166.
(38) Li, J.; Ma, Y. In-Situ Synthesis of Transparent Conductive PEDOT Coating on PET Foil by Liquid Phase Depositional Polymerization of EDOT. *Synth. Met.* **2016**, *217*, 185–188.
(39) Li, J.-X.; Ma, Y.-X. Study on Fabricating PEDOT Electrodes by Liquid Phase Depositional Polymerization of EDOT and Direct Patterning with 172 nm Vacuum Ultraviolet Radiation. *ACS Appl. Energy Mater.* **2018**, *1* (1), 134–142.
(40) Bhattacharyya, D.; Howden, R. M.; Borrelli, D. C.; Gleason, K. K. Vapor Phase Oxidative Synthesis of Conjugated Polymers and Applications. *J. Polym. Sci. Part B Polym. Phys.* **2012**, *50* (19), 1329–1351.
(41) Chelawat, H.; Vaddiraju, S.; Gleason, K. Conformal, Conducting Poly(3,4-ethylenedioxythiophene) Thin Films Deposited Using Bromine as the Oxidant in a Completely Dry Oxidative Chemical Vapor Deposition Process. *Chem. Mater.* **2010**, 22 (9), 2864–2868.
(42) Lee, S.; Gleason, K. K. Enhanced Optical Property with Tunable Band Gap of Cross-Linked PEDOT Copolymers via Oxidative Chemical Vapor Deposition. *Adv. Funct. Mater.* **2015**, *25* (1), 85–93.
(43) Fabretto, M.; Zuber, K.; Hall, C.; Murphy, P. High Conductivity PEDOT Using Humidity Facilitated Vacuum Vapour Phase Polymerisation. *Macromol. Rapid Commun.* **2008**, *29* (16), 1403–1409.
(44) Fabretto, M.; Autere, J.-P.; Hoglinger, D.; Field, S.; Murphy, P. Vacuum vapour phase polymerised poly(3,4-ethyelendioxythiophene) thin films for use in large-scale electrochromic devices. *Thin Solid Films* **2011**, 519 (8), 2544–2549.

(45) Kim, J.; Kim, E.; Won, Y.; Lee, H.; Suh, K. The Preparation and Characteristics of Conductive Poly(3,4-Ethylenedioxythiophene) Thin Film by Vapor-Phase Polymerization. *Synth. Met.* **2003**, *139* (2), 485–489.
(46) Winther-Jensen, B.; Forsyth, M.; West, K.; Andreasen, J. W.; Bayley, P.; Pas, S.; MacFarlane, D. R. Order–Disorder Transitions in Poly(3,4-Ethylenedioxythiophene). *Polymer* **2008**, *49* (2), 481–487.
(47) Fabretto, M.; Jariego-Moncunill, C.; Autere, J.-P.; Michelmore, A.; Short, R. D.; Murphy, P. High Conductivity PEDOT Resulting from Glycol/Oxidant Complex and Glycol/Polymer Intercalation during Vacuum Vapour Phase Polymerisation. *Polymer* **2011**, *52* (8), 1725–1730.
(48) Mueller, M.; Fabretto, M.; Evans, D.; Hojati-Talemi, P.; Gruber, C.; Murphy, P. Vacuum Vapour Phase Polymerization of High Conductivity PEDOT: Role of PEG-PPG-PEG, the Origin of Water, and Choice of Oxidant. *Polymer* **2012**, *53* (11), 2146–2151.
(49) Winther-Jensen, B.; West, K. Stability of Highly Conductive Poly-3,4-Ethylenedioxythiophene. *React. Funct. Polym.* **2006**, *66* (5), 479–483.
(50) Madl, C. M.; Kariuki, P. N.; Gendron, J.; Piper, L. F. J.; Jones, W. E. Vapor Phase Polymerization of Poly (3,4-Ethylenedioxythiophene) on Flexible Substrates for Enhanced Transparent Electrodes. *Synth. Met.* **2011**, *161* (13), 1159–1165.
(51) Howden, R. M.; McVay, E. D.; Gleason, K. K. oCVD Poly(3,4-Ethylenedioxythiophene) Conductivity and Lifetime Enhancement via Acid Rinse Dopant Exchange. *J. Mater. Chem. A* **2012**, *1* (4), 1334–1340.
(52) Fan, F.-R.; Tian, Z.-Q.; Lin Wang, Z. Flexible Triboelectric Generator. *Nano Energy* **2012**, *1* (2), 328–334.
(53) Wang, Y.; Yang, Y.; Wang, Z. L. Triboelectric Nanogenerators as Flexible Power Sources. *npj Flex. Electron.* **2017**, *1* (1), 10.
(54) Šutka, A.; Timusk, M.; Metsik, J.; Ruža, J.; Knite, M.; Mäeorg, U. PEDOT Electrodes for Triboelectric Generator Devices. *Org. Electron.* **2017**, *51*, 446–451.
(55) Galembeck, F.; L. Burgo, T. A.; S. Balestrin, L. B.; F. Gouveia, R.; A. Silva, C.; Galembeck, A. Friction, Tribochemistry and Triboelectricity: Recent Progress and Perspectives. *RSC Adv.* **2014**, *4* (109), 64280–64298.
(56) Diaz, A. F.; Felix-Navarro, R. M. A Semi-Quantitative Tribo-Electric Series for Polymeric Materials: The Influence of Chemical Structure and Properties. *J. Electrost.* **2004**, *62* (4), 277–290.
(57) Baytekin, H. T.; Patashinski, A. Z.; Branicki, M.; Baytekin, B.; Soh, S.; Grzybowski, B. A. The Mosaic of Surface Charge in Contact Electrification. *Science* **2011**, *333* (6040), 308–312.
(58) Baytekin, H. T.; Baytekin, B.; Incorvati, J. T.; Grzybowski, B. A. Material Transfer and Polarity Reversal in Contact Charging. *Angew. Chem. Int. Ed.* **2012**, *51* (20), 4843–4847.
(59) Lin Wang, Z.; Chen, J.; Lin, L. Progress in Triboelectric Nanogenerators as a New Energy Technology and Self-Powered Sensors. *Energy Environ. Sci.* **2015**, *8* (8), 2250–2282.
(60) Lin Wang, Z. Triboelectric Nanogenerators as New Energy Technology and Self-Powered Sensors – Principles, Problems and Perspectives. *Faraday Discuss.* **2014**, *176* (0), 447–458.

(61) Zhu, G.; Peng, B.; Chen, J.; Jing, Q.; Lin Wang, Z. Triboelectric Nanogenerators as a New Energy Technology: From Fundamentals, Devices, to Applications. *Nano Energy* **2015**, *14*, 126–138.
(62) Metsik, J.; Saal, K.; Mäeorg, U.; Lõhmus, R.; Leinberg, S.; Mändar, H.; Kodu, M.; Timusk, M. Growth of Poly(3,4-Ethylenedioxythiophene) Films Prepared by Base-Inhibited Vapor Phase Polymerization. *J. Polym. Sci. Part B Polym. Phys.* **2014**, *52* (8), 561–571.
(63) Logan, M. A. Sheet Resistivity Measurements on Rectangular Surfaces-General Solution for Four Point Probe Conversion Factors. *Bell Syst. Tech. J.* **1967**, *46* (10), 2277–2322.
(64) Park, B.; Yang, L.; Johansson, E. M. J.; Vlachopoulos, N.; Chams, A.; Perruchot, C.; Jouini, M.; Boschloo, G.; Hagfeldt, A. Neutral, Polaron, and Bipolaron States in PEDOT Prepared by Photoelectrochemical Polymerization and the Effect on Charge Generation Mechanism in the Solid-State Dye-Sensitized Solar Cell. *J. Phys. Chem. C* **2013**, *117* (44), 22484–22491.
(65) Sixou, B.; Mermilliod, N.; Travers, J. P. Aging Effects on the Transport Properties in Conducting Polymer Polypyrrole. *Phys. Rev. B* **1996**, *53* (8), 4509–4521.
(66) Rannou, P.; Nechtschein, M. Ageing of Poly(3,4-ethylenedioxythiophene): Kinetics of conductivity decay and lifespan. *Synth. Met.* **1999**, *101* (1–3), 474.
(67) Marciniak, S.; Crispin, X.; Uvdal, K.; Trzcinski, M.; Birgerson, J.; Groenendaal, L.; Louwet, F.; Salaneck, W. R. Light induced damage in poly(3,4-ethylenedioxythiophene) and its derivatives studied by photoelectron spectroscopy. *Synth. Met.* **2004**, *141* (1–2), 67–73.
(68) Garreau, S.; Louarn, G.; Buisson, J. P.; Froyer, G.; Lefrant, S. In Situ Spectroelectrochemical Raman Studies of Poly(3,4-Ethylenedioxythiophene) (PEDT). *Macromolecules* **1999**, *32* (20), 6807–6812.
(69) Kok, M. M. de; Buechel, M.; Vulto, S. I. E.; Weijer, P. van de; Meulenkamp, E. A.; Winter, S. H. P. M. de; Mank, A. J. G.; Vorstenbosch, H. J. M.; Weijtens, C. H. L.; Elsbergen, V. van. Modification of PEDOT:PSS as Hole Injection Layer in Polymer LEDs. *Phys. Status Solidi A* **2004**, *201* (6), 1342–1359.
(70) Zhu, G.; Lin, Z.-H.; Jing, Q.; Bai, P.; Pan, C.; Yang, Y.; Zhou, Y.; Wang, Z. L. Toward Large-Scale Energy Harvesting by a Nanoparticle-Enhanced Triboelectric Nanogenerator. *Nano Lett.* **2013**, *13* (2), 847–853.

SUMMARY IN ESTONIAN

Polü(3,4-etüleendioksütiofeeni) õhukeste kilede valmistamine ja stabiilsus rakendusteks läbipaistva elektroodina

Polümerisatsioon gaasifaasist (VPP) ja vedelfaasilise sadestamise polümerisatsioon (LPDP) on kaks erinevat oksüdatiivse polümeristsiooni meetodit mida kasutati käesolevas töös elektrit juhtiva polümeeri polü(3,4-etüleendioksütiofeeni) (PEDOT) kilede valmistamiseks. VPP käigus valmistati suhteliselt kõrge juhtivusega ja läbipaistvusega PEDOTi kiled (550 nm juures 90% läbilaskvus ja pindtakistus alla 300 Ω/ruut). Parimad juhtivuse väärtused ületasid 1300 S/cm. Uuriti temperatuuri, kasvuaja, oksüdeerija lahuse kontsentratsiooni ja suhtelise õhuniiskuse mõju kilede optilistele ja elektrilistele omadustele ning määrati kilede valmistamiseks sobilikud tingimused. Täheldati kolme erinevat kasvustaadiumit, mis andsid erinevate omadustega kiled. Valmistamisjärgselt põhjustas varases kasvustaadiumis PEDOTi/oksüdeerija kilede pesemine suure takistuse languse, mis viitab PEDOTi nodulaarsele kasvule kile moodustumisel.

Võrreldes VPPga andis LPDP madalamate juhtivustega kiled, millel oli defektne pinna mikrostruktuur. *In situ* läbilaskvuse mõõtmised kombineeriti samaaegsete *in situ* takistuse mõõtmistega, et saada polümerisatsiooniprotsessist paremat ülevaadet. Avastati, et see oli kolmeastmeline ja meenutas VPP protsessi.

In situ takistuse mõõtmiste abil hinnati VPP PEDOTi kilede stabiilsust nii toatemperatuuril kui ka kõrgendatud temperatuuridel erinevates gaasikeskkondades. PEDOT oli suhteliselt stabiilne kuivades ja pimedates keskkondades toatemperatuuril, kuigi ka siis esines väike lineaarne takistuse kasv (~4–5% 10 päeva kohta). UV-valguse, veeauru ja üllatuslikult ka vaakumi mõjul toimus toatemperatuuril kiirem takistuse kasv. Vananemist kiirendati ka temperatuuri tõstmisega kuni väärtuseni 140 °C ja nii inertgaasi kui õhu keskkonnas toimus vananemine kõrgendatud temperatuuril sarnaselt. Iseloomulikud muutused UV-Vis-NIR neeldumisspektris näitavad polaronide ja bipolaronide olekute jaotuse muutust materjalis. Madaltemperatuursed takistuse mõõtmised näitasid, et kui värskelt valmistatud PEDOTi kiled on juhtivuse kriitilises režiimis metall-isolaator siirde juures, siis termiliselt vanandatud kilede juhtivus on isoleerivas režiimis kirjeldatav 2-D või 3-D Motti mudeli abil.

PEDOTi kilesid kasutati korraga nii kontaktpinnana kui ka elektroodina triboelektrilises nanogeneraatoris mehaanilise energia elektrienergiaks muundamiseks. VPP PEDOT oli sellises rakenduses parem kui indiumtinaoksiid, võimaldades ~3 korda kõrgemat võimsustihedust. VPP PEDOTi sisaldav seade oli stabiilne rohkem kui 1000 tsüklit, mis näitab PEDOTi sobilikkust selleks rakenduseks.

ACKNOWLEDGEMENTS

I would like to thank my supervisor Uno Mäeorg for guidance and interesting discussions and supervisor Martin Timusk for useful ideas, development of several experimental setups and help with experimental techniques.

I appreciate the invaluable contribution of the co-authors of my research papers. Also, I am grateful to all the people who additionally helped with the measurements: Madis Lobjakas for developing accelerated aging system for inert gas environment, Mikk Vahtrus for help with low-temperature resistance measurements, Kadri Savi for calculating correction factors for four-point probe measurements, Mikk Antsov for performing some AFM measurements and Aigi Salundi for preparation of films by sol-gel technique.

I am thankful to all the present and former members of my research groups in Institute of Chemistry and Institute of Physics.

I am grateful to my mother, friends and relatives for supporting me. My special gratitude belongs to Sigrid Rand for proofreading the manuscript.

Also, I would like to thank my chemistry teacher Maila Mölder, who sparked my interest in chemistry.

This research was supported by institutional research funding project IUT20-17 of the Estonian Ministry of Education, Estonian Centre of Excellence in Zero Energy and Resource Efficient Smart Buildings and Districts, ZEBE, grant 2014-2020.4.01.15-0016 funded by the European Regional Development Fund. This work was also supported by Graduate School of Functional materials and technologies receiving funding from the European Regional Development Fund in University of Tartu, Estonia.

PUBLICATIONS

CURRICULUM VITAE

Name: Jörgen Metsik
Date of birth: February 25, 1989
Citizenship: Estonian
Address: Institute of Chemistry, Faculty of Science and Technology, University of Tartu, Ravila 14A, 50411, Tartu, Estonia
E-mail: jorgen.metsik@ut.ee

Education:

2013–present	University of Tartu, PhD student in chemistry
2011–2013	University of Tartu, MSc in chemistry, *cum laude*
2008–2011	University of Tartu, BSc in chemistry, *cum laude*
1996–2008	Tallinn Järveotsa Gymnasium

Professional employment:

01.11.2016–31.08.2017	University of Tartu, Junior Research Fellow (0.15)
01.04.2014–31.12.2014	University of Tartu, Specialist (0.60)
01.03.2013–31.03.2014	University of Tartu, Specialist (0.70)
01.09.2012–28.02.2013	University of Tartu, Specialist (0.80)

Scientific publications:

1. Metsik, J.; Timusk M.; Šutka, A.; Mooste, M.; Tammeveski K.; Mäeorg, U. *In situ* investigation of poly(3,4-ethylenedioxythiophene) film growth during liquid phase deposition polymerization. *Thin Solid Films* **2018**, *653*, 274–283.
2. Šutka, A.; Timusk, M.; Metsik, J.; Ruža, J.; Knite, M.; Mäeorg, U. PEDOT Electrodes for Triboelectric Generator Devices. *Org. Electron.* **2017**, *51*, 446–451.
3. Metsik, J.; Timusk, M.; Käämbre, T.; Mändar, H; Umalas, M.; Kuus, A.; Puust, L.; Utt, K.; Sildos, I.; Mäeorg, U. Stability of poly(3,4-ethylenedioxythiophene) thin films prepared by vapor phase polymerization. *Polym. Degrad. Stab.* **2016**, *126*, 170–178.
4. Metsik, J.; Saal, K.; Mäeorg, U.; Lõhmus, R.; Leinberg, S; Mändar, H.; Kodu, M.; Timusk, M. Growth of Poly(3,4-ethylenedioxythiophene) Films Prepared by Base-Inhibited Vapor Phase Polymerization. *J. Polym. Sci. Part B: Polym. Phys.* **2014**, *52*, 561–571.

ELULOOKIRJELDUS

Nimi: Jörgen Metsik
Sünniaeg: 25. veebruar 1989
Kodakondsus: Eesti
Aadress: Keemia Instituut, Loodus- ja täppisteaduste valdkond, Tartu Ülikool, Ravila 14A, 50411, Tartu, Eesti
E-mail: jorgen.metsik@ut.ee

Haridus:

2013–praegu	Tartu Ülikool, keemia doktorantuur
2011–2013	Tartu Ülikool, keemia magistriõpe, *cum laude*
2008–2011	Tartu Ülikool, keemia bakalureuseõpe, *cum laude*
1996–2008	Tallinna Järveotsa Gümnaasium

Teenistuskäik:

01.11.2016–31.08.2017	Tartu Ülikool, nooremteadur (0,15)
01.04.2014–31.12.2014	Tartu Ülikool, spetsialist (0,60)
01.03.2013–31.03.2014	Tartu Ülikool, spetsialist (0,70)
01.09.2012–28.02.2013	Tartu Ülikool, spetsialist (0,80)

Teaduspublikatsioonid:

1. Metsik, J.; Timusk, M.; Šutka, A.; Mooste, M.; Tammeveski K.; Mäeorg, U. *In situ* investigation of poly(3,4-ethylenedioxythiophene) film growth during liquid phase deposition polymerization. *Thin Solid Films* **2018**, *653*, 274–283.
2. Šutka, A.; Timusk, M.; Metsik, J.; Ruža, J.; Knite, M.; Mäeorg, U. PEDOT Electrodes for Triboelectric Generator Devices. *Org. Electron.* **2017**, *51*, 446–451.
3. Metsik, J.; Timusk, M.; Käämbre, T.; Mändar, H; Umalas, M.; Kuus, A.; Puust, L.; Utt, K.; Sildos, I.; Mäeorg, U. Stability of poly(3,4-ethylenedioxythiophene) thin films prepared by vapor phase polymerization. *Polym. Degrad. Stab.* **2016**, *126*, 170–178.
4. Metsik, J.; Saal, K.; Mäeorg, U.; Lõhmus, R.; Leinberg, S; Mändar, H.; Kodu, M.; Timusk, M. Growth of Poly(3,4-ethylenedioxythiophene) Films Prepared by Base-Inhibited Vapor Phase Polymerization. *J. Polym. Sci Part B: Polym. Phys.* **2014**, *52*, 561–571.

DISSERTATIONES CHIMICAE UNIVERSITATIS TARTUENSIS

1. **Toomas Tamm.** Quantum-chemical simulation of solvent effects. Tartu, 1993, 110 p.
2. **Peeter Burk.** Theoretical study of gas-phase acid-base equilibria. Tartu, 1994, 96 p.
3. **Victor Lobanov.** Quantitative structure-property relationships in large descriptor spaces. Tartu, 1995, 135 p.
4. **Vahur Mäemets.** The ^{17}O and ^{1}H nuclear magnetic resonance study of H_2O in individual solvents and its charged clusters in aqueous solutions of electrolytes. Tartu, 1997, 140 p.
5. **Andrus Metsala.** Microcanonical rate constant in nonequilibrium distribution of vibrational energy and in restricted intramolecular vibrational energy redistribution on the basis of slater's theory of unimolecular reactions. Tartu, 1997, 150 p.
6. **Uko Maran.** Quantum-mechanical study of potential energy surfaces in different environments. Tartu, 1997, 137 p.
7. **Alar Jänes.** Adsorption of organic compounds on antimony, bismuth and cadmium electrodes. Tartu, 1998, 219 p.
8. **Kaido Tammeveski.** Oxygen electroreduction on thin platinum films and the electrochemical detection of superoxide anion. Tartu, 1998, 139 p.
9. **Ivo Leito.** Studies of Brønsted acid-base equilibria in water and non-aqueous media. Tartu, 1998, 101 p.
10. **Jaan Leis.** Conformational dynamics and equilibria in amides. Tartu, 1998, 131 p.
11. **Toonika Rinken.** The modelling of amperometric biosensors based on oxidoreductases. Tartu, 2000, 108 p.
12. **Dmitri Panov.** Partially solvated Grignard reagents. Tartu, 2000, 64 p.
13. **Kaja Orupõld.** Treatment and analysis of phenolic wastewater with microorganisms. Tartu, 2000, 123 p.
14. **Jüri Ivask.** Ion Chromatographic determination of major anions and cations in polar ice core. Tartu, 2000, 85 p.
15. **Lauri Vares.** Stereoselective Synthesis of Tetrahydrofuran and Tetrahydropyran Derivatives by Use of Asymmetric Horner-Wadsworth-Emmons and Ring Closure Reactions. Tartu, 2000, 184 p.
16. **Martin Lepiku.** Kinetic aspects of dopamine D_2 receptor interactions with specific ligands. Tartu, 2000, 81 p.
17. **Katrin Sak.** Some aspects of ligand specificity of P2Y receptors. Tartu, 2000, 106 p.
18. **Vello Pällin.** The role of solvation in the formation of iotsitch complexes. Tartu, 2001, 95 p.
19. **Katrin Kollist.** Interactions between polycyclic aromatic compounds and humic substances. Tartu, 2001, 93 p.

20. **Ivar Koppel.** Quantum chemical study of acidity of strong and superstrong Brønsted acids. Tartu, 2001, 104 p.
21. **Viljar Pihl.** The study of the substituent and solvent effects on the acidity of OH and CH acids. Tartu, 2001, 132 p.
22. **Natalia Palm.** Specification of the minimum, sufficient and significant set of descriptors for general description of solvent effects. Tartu, 2001, 134 p.
23. **Sulev Sild.** QSPR/QSAR approaches for complex molecular systems. Tartu, 2001, 134 p.
24. **Ruslan Petrukhin.** Industrial applications of the quantitative structure-property relationships. Tartu, 2001, 162 p.
25. **Boris V. Rogovoy.** Synthesis of (benzotriazolyl)carboximidamides and their application in relations with *N*- and *S*-nucleophyles. Tartu, 2002, 84 p.
26. **Koit Herodes.** Solvent effects on UV-vis absorption spectra of some solvatochromic substances in binary solvent mixtures: the preferential solvation model. Tartu, 2002, 102 p.
27. **Anti Perkson.** Synthesis and characterisation of nanostructured carbon. Tartu, 2002, 152 p.
28. **Ivari Kaljurand.** Self-consistent acidity scales of neutral and cationic Brønsted acids in acetonitrile and tetrahydrofuran. Tartu, 2003, 108 p.
29. **Karmen Lust.** Adsorption of anions on bismuth single crystal electrodes. Tartu, 2003, 128 p.
30. **Mare Piirsalu.** Substituent, temperature and solvent effects on the alkaline hydrolysis of substituted phenyl and alkyl esters of benzoic acid. Tartu, 2003, 156 p.
31. **Meeri Sassian.** Reactions of partially solvated Grignard reagents. Tartu, 2003, 78 p.
32. **Tarmo Tamm.** Quantum chemical modelling of polypyrrole. Tartu, 2003. 100 p.
33. **Erik Teinemaa.** The environmental fate of the particulate matter and organic pollutants from an oil shale power plant. Tartu, 2003. 102 p.
34. **Jaana Tammiku-Taul.** Quantum chemical study of the properties of Grignard reagents. Tartu, 2003. 120 p.
35. **Andre Lomaka.** Biomedical applications of predictive computational chemistry. Tartu, 2003. 132 p.
36. **Kostyantyn Kirichenko.** Benzotriazole – Mediated Carbon–Carbon Bond Formation. Tartu, 2003. 132 p.
37. **Gunnar Nurk.** Adsorption kinetics of some organic compounds on bismuth single crystal electrodes. Tartu, 2003, 170 p.
38. **Mati Arulepp.** Electrochemical characteristics of porous carbon materials and electrical double layer capacitors. Tartu, 2003, 196 p.
39. **Dan Cornel Fara.** QSPR modeling of complexation and distribution of organic compounds. Tartu, 2004, 126 p.
40. **Riina Mahlapuu.** Signalling of galanin and amyloid precursor protein through adenylate cyclase. Tartu, 2004, 124 p.

41. **Mihkel Kerikmäe.** Some luminescent materials for dosimetric applications and physical research. Tartu, 2004, 143 p.
42. **Jaanus Kruusma.** Determination of some important trace metal ions in human blood. Tartu, 2004, 115 p.
43. **Urmas Johanson.** Investigations of the electrochemical properties of polypyrrole modified electrodes. Tartu, 2004, 91 p.
44. **Kaido Sillar.** Computational study of the acid sites in zeolite ZSM-5. Tartu, 2004, 80 p.
45. **Aldo Oras.** Kinetic aspects of dATPαS interaction with $P2Y_1$ receptor. Tartu, 2004, 75 p.
46. **Erik Mölder.** Measurement of the oxygen mass transfer through the air-water interface. Tartu, 2005, 73 p.
47. **Thomas Thomberg.** The kinetics of electroreduction of peroxodisulfate anion on cadmium (0001) single crystal electrode. Tartu, 2005, 95 p.
48. **Olavi Loog.** Aspects of condensations of carbonyl compounds and their imine analogues. Tartu, 2005, 83 p.
49. **Siim Salmar.** Effect of ultrasound on ester hydrolysis in aqueous ethanol. Tartu, 2006, 73 p.
50. **Ain Uustare.** Modulation of signal transduction of heptahelical receptors by other receptors and G proteins. Tartu, 2006, 121 p.
51. **Sergei Yurchenko.** Determination of some carcinogenic contaminants in food. Tartu, 2006, 143 p.
52. **Kaido Tämm.** QSPR modeling of some properties of organic compounds. Tartu, 2006, 67 p.
53. **Olga Tšubrik.** New methods in the synthesis of multisubstituted hydrazines. Tartu. 2006, 183 p.
54. **Lilli Sooväli.** Spectrophotometric measurements and their uncertainty in chemical analysis and dissociation constant measurements. Tartu, 2006, 125 p.
55. **Eve Koort.** Uncertainty estimation of potentiometrically measured ph and pK_a values. Tartu, 2006, 139 p.
56. **Sergei Kopanchuk.** Regulation of ligand binding to melanocortin receptor subtypes. Tartu, 2006, 119 p.
57. **Silvar Kallip.** Surface structure of some bismuth and antimony single crystal electrodes. Tartu, 2006, 107 p.
58. **Kristjan Saal.** Surface silanization and its application in biomolecule coupling. Tartu, 2006, 77 p.
59. **Tanel Tätte.** High viscosity $Sn(OBu)_4$ oligomeric concentrates and their applications in technology. Tartu, 2006, 91 p.
60. **Dimitar Atanasov Dobchev**. Robust QSAR methods for the prediction of properties from molecular structure. Tartu, 2006, 118 p.
61. **Hannes Hagu**. Impact of ultrasound on hydrophobic interactions in solutions. Tartu, 2007, 81 p.
62. **Rutha Jäger.** Electroreduction of peroxodisulfate anion on bismuth electrodes. Tartu, 2007, 142 p.

63. **Kaido Viht.** Immobilizable bisubstrate-analogue inhibitors of basophilic protein kinases: development and application in biosensors. Tartu, 2007, 88 p.
64. **Eva-Ingrid Rõõm.** Acid-base equilibria in nonpolar media. Tartu, 2007, 156 p.
65. **Sven Tamp.** DFT study of the cesium cation containing complexes relevant to the cesium cation binding by the humic acids. Tartu, 2007, 102 p.
66. **Jaak Nerut.** Electroreduction of hexacyanoferrate(III) anion on Cadmium (0001) single crystal electrode. Tartu, 2007, 180 p.
67. **Lauri Jalukse.** Measurement uncertainty estimation in amperometric dissolved oxygen concentration measurement. Tartu, 2007, 112 p.
68. **Aime Lust.** Charge state of dopants and ordered clusters formation in CaF_2:Mn and CaF_2:Eu luminophors. Tartu, 2007, 100 p.
69. **Iiris Kahn**. Quantitative Structure-Activity Relationships of environmentally relevant properties. Tartu, 2007, 98 p.
70. **Mari Reinik.** Nitrates, nitrites, N-nitrosamines and polycyclic aromatic hydrocarbons in food: analytical methods, occurrence and dietary intake. Tartu, 2007, 172 p.
71. **Heili Kasuk.** Thermodynamic parameters and adsorption kinetics of organic compounds forming the compact adsorption layer at Bi single crystal electrodes. Tartu, 2007, 212 p.
72. **Erki Enkvist.** Synthesis of adenosine-peptide conjugates for biological applications. Tartu, 2007, 114 p.
73. **Svetoslav Hristov Slavov**. Biomedical applications of the QSAR approach. Tartu, 2007, 146 p.
74. **Eneli Härk.** Electroreduction of complex cations on electrochemically polished Bi(*hkl*) single crystal electrodes. Tartu, 2008, 158 p.
75. **Priit Möller.** Electrochemical characteristics of some cathodes for medium temperature solid oxide fuel cells, synthesized by solid state reaction technique. Tartu, 2008, 90 p.
76. **Signe Viggor.** Impact of biochemical parameters of genetically different pseudomonads at the degradation of phenolic compounds. Tartu, 2008, 122 p.
77. **Ave Sarapuu.** Electrochemical reduction of oxygen on quinone-modified carbon electrodes and on thin films of platinum and gold. Tartu, 2008, 134 p.
78. **Agnes Kütt.** Studies of acid-base equilibria in non-aqueous media. Tartu, 2008, 198 p.
79. **Rouvim Kadis.** Evaluation of measurement uncertainty in analytical chemistry: related concepts and some points of misinterpretation. Tartu, 2008, 118 p.
80. **Valter Reedo.** Elaboration of IVB group metal oxide structures and their possible applications. Tartu, 2008, 98 p.
81. **Aleksei Kuznetsov.** Allosteric effects in reactions catalyzed by the cAMP-dependent protein kinase catalytic subunit. Tartu, 2009, 133 p.

82. **Aleksei Bredihhin.** Use of mono- and polyanions in the synthesis of multisubstituted hydrazine derivatives. Tartu, 2009, 105 p.
83. **Anu Ploom.** Quantitative structure-reactivity analysis in organosilicon chemistry. Tartu, 2009, 99 p.
84. **Argo Vonk.** Determination of adenosine A_{2A}- and dopamine D_1 receptor-specific modulation of adenylate cyclase activity in rat striatum. Tartu, 2009, 129 p.
85. **Indrek Kivi.** Synthesis and electrochemical characterization of porous cathode materials for intermediate temperature solid oxide fuel cells. Tartu, 2009, 177 p.
86. **Jaanus Eskusson.** Synthesis and characterisation of diamond-like carbon thin films prepared by pulsed laser deposition method. Tartu, 2009, 117 p.
87. **Marko Lätt.** Carbide derived microporous carbon and electrical double layer capacitors. Tartu, 2009, 107 p.
88. **Vladimir Stepanov.** Slow conformational changes in dopamine transporter interaction with its ligands. Tartu, 2009, 103 p.
89. **Aleksander Trummal.** Computational Study of Structural and Solvent Effects on Acidities of Some Brønsted Acids. Tartu, 2009, 103 p.
90. **Eerold Vellemäe.** Applications of mischmetal in organic synthesis. Tartu, 2009, 93 p.
91. **Sven Parkel.** Ligand binding to 5-HT_{1A} receptors and its regulation by Mg^{2+} and Mn^{2+}. Tartu, 2010, 99 p.
92. **Signe Vahur.** Expanding the possibilities of ATR-FT-IR spectroscopy in determination of inorganic pigments. Tartu, 2010, 184 p.
93. **Tavo Romann**. Preparation and surface modification of bismuth thin film, porous, and microelectrodes. Tartu, 2010, 155 p.
94. **Nadežda Aleksejeva.** Electrocatalytic reduction of oxygen on carbon nanotube-based nanocomposite materials. Tartu, 2010, 147 p.
95. **Marko Kullapere.** Electrochemical properties of glassy carbon, nickel and gold electrodes modified with aryl groups. Tartu, 2010, 233 p.
96. **Liis Siinor.** Adsorption kinetics of ions at Bi single crystal planes from aqueous electrolyte solutions and room-temperature ionic liquids. Tartu, 2010, 101 p.
97. **Angela Vaasa.** Development of fluorescence-based kinetic and binding assays for characterization of protein kinases and their inhibitors. Tartu 2010, 101 p.
98. **Indrek Tulp.** Multivariate analysis of chemical and biological properties. Tartu 2010, 105 p.
99. **Aare Selberg.** Evaluation of environmental quality in Northern Estonia by the analysis of leachate. Tartu 2010, 117 p.
100. **Darja Lavõgina.** Development of protein kinase inhibitors based on adenosine analogue-oligoarginine conjugates. Tartu 2010, 248 p.
101. **Laura Herm.** Biochemistry of dopamine D_2 receptors and its association with motivated behaviour. Tartu 2010, 156 p.

102. **Terje Raudsepp.** Influence of dopant anions on the electrochemical properties of polypyrrole films. Tartu 2010, 112 p.
103. **Margus Marandi.** Electroformation of Polypyrrole Films: *In-situ* AFM and STM Study. Tartu 2011, 116 p.
104. **Kairi Kivirand.** Diamine oxidase-based biosensors: construction and working principles. Tartu, 2011, 140 p.
105. **Anneli Kruve.** Matrix effects in liquid-chromatography electrospray mass-spectrometry. Tartu, 2011, 156 p.
106. **Gary Urb.** Assessment of environmental impact of oil shale fly ash from PF and CFB combustion. Tartu, 2011, 108 p.
107. **Nikita Oskolkov.** A novel strategy for peptide-mediated cellular delivery and induction of endosomal escape. Tartu, 2011, 106 p.
108. **Dana Martin.** The QSPR/QSAR approach for the prediction of properties of fullerene derivatives. Tartu, 2011, 98 p.
109. **Säde Viirlaid.** Novel glutathione analogues and their antioxidant activity. Tartu, 2011, 106 p.
110. **Ülis Sõukand.** Simultaneous adsorption of Cd^{2+}, Ni^{2+}, and Pb^{2+} on peat. Tartu, 2011, 124 p.
111. **Lauri Lipping.** The acidity of strong and superstrong Brønsted acids, an outreach for the "limits of growth": a quantum chemical study. Tartu, 2011, 124 p.
112. **Heisi Kurig.** Electrical double-layer capacitors based on ionic liquids as electrolytes. Tartu, 2011, 146 p.
113. **Marje Kasari.** Bisubstrate luminescent probes, optical sensors and affinity adsorbents for measurement of active protein kinases in biological samples. Tartu, 2012, 126 p.
114. **Kalev Takkis.** Virtual screening of chemical databases for bioactive molecules. Tartu, 2012, 122 p.
115. **Ksenija Kisseljova**. Synthesis of aza-β^3-amino acid containing peptides and kinetic study of their phosphorylation by protein kinase A. Tartu, 2012, 104 p.
116. **Riin Rebane.** Advanced method development strategy for derivatization LC/ESI/MS. Tartu, 2012, 184 p.
117. **Vladislav Ivaništšev.** Double layer structure and adsorption kinetics of ions at metal electrodes in room temperature ionic liquids. Tartu, 2012, 128 p.
118. **Irja Helm.** High accuracy gravimetric Winkler method for determination of dissolved oxygen. Tartu, 2012, 139 p.
119. **Karin Kipper.** Fluoroalcohols as Components of LC-ESI-MS Eluents: Usage and Applications. Tartu, 2012, 164 p.
120. **Arno Ratas.** Energy storage and transfer in dosimetric luminescent materials. Tartu, 2012, 163 p.
121. **Reet Reinart-Okugbeni**. Assay systems for characterisation of subtype-selective binding and functional activity of ligands on dopamine receptors. Tartu, 2012, 159 p.

122. **Lauri Sikk.** Computational study of the Sonogashira cross-coupling reaction. Tartu, 2012, 81 p.
123. **Karita Raudkivi.** Neurochemical studies on inter-individual differences in affect-related behaviour of the laboratory rat. Tartu, 2012, 161 p.
124. **Indrek Saar.** Design of GalR2 subtype specific ligands: their role in depression-like behavior and feeding regulation. Tartu, 2013, 126 p.
125. **Ann Laheäär.** Electrochemical characterization of alkali metal salt based non-aqueous electrolytes for supercapacitors. Tartu, 2013, 127 p.
126. **Kerli Tõnurist.** Influence of electrospun separator materials properties on electrochemical performance of electrical double-layer capacitors. Tartu, 2013, 147 p.
127. **Kaija Põhako-Esko.** Novel organic and inorganic ionogels: preparation and characterization. Tartu, 2013, 124 p.
128. **Ivar Kruusenberg.** Electroreduction of oxygen on carbon nanomaterial-based catalysts. Tartu, 2013, 191 p.
129. **Sander Piiskop.** Kinetic effects of ultrasound in aqueous acetonitrile solutions. Tartu, 2013, 95 p.
130. **Ilona Faustova**. Regulatory role of L-type pyruvate kinase N-terminal domain. Tartu, 2013, 109 p.
131. **Kadi Tamm.** Synthesis and characterization of the micro-mesoporous anode materials and testing of the medium temperature solid oxide fuel cell single cells. Tartu, 2013, 138 p.
132. **Iva Bozhidarova Stoyanova-Slavova.** Validation of QSAR/QSPR for regulatory purposes. Tartu, 2013, 109 p.
133. **Vitali Grozovski**. Adsorption of organic molecules at single crystal electrodes studied by *in situ* STM method. Tartu, 2014, 146 p.
134. **Santa Veikšina**. Development of assay systems for characterisation of ligand binding properties to melanocortin 4 receptors. Tartu, 2014, 151 p.
135. **Jüri Liiv.** PVDF (polyvinylidene difluoride) as material for active element of twisting-ball displays. Tartu, 2014, 111 p.
136. **Kersti Vaarmets.** Electrochemical and physical characterization of pristine and activated molybdenum carbide-derived carbon electrodes for the oxygen electroreduction reaction. Tartu, 2014, 131 p.
137. **Lauri Tõntson**. Regulation of G-protein subtypes by receptors, guanine nucleotides and Mn^{2+}. Tartu, 2014, 105 p.
138. **Aiko Adamson.** Properties of amine-boranes and phosphorus analogues in the gas phase. Tartu, 2014, 78 p.
139. **Elo Kibena**. Electrochemical grafting of glassy carbon, gold, highly oriented pyrolytic graphite and chemical vapour deposition-grown graphene electrodes by diazonium reduction method. Tartu, 2014, 184 p.
140. **Teemu Näykki.** Novel Tools for Water Quality Monitoring – From Field to Laboratory. Tartu, 2014, 202 p.
141. **Karl Kaupmees.** Acidity and basicity in non-aqueous media: importance of solvent properties and purity. Tartu, 2014, 128 p.

142. **Oleg Lebedev**. Hydrazine polyanions: different strategies in the synthesis of heterocycles. Tartu, 2015, 118 p.
143. **Geven Piir.** Environmental risk assessment of chemicals using QSAR methods. Tartu, 2015, 123 p.
144. **Olga Mazina.** Development and application of the biosensor assay for measurements of cyclic adenosine monophosphate in studies of G protein-coupled receptor signalinga. Tartu, 2015, 116 p.
145. **Sandip Ashokrao Kadam.** Anion receptors: synthesis and accurate binding measurements. Tartu, 2015, 116 p.
146. **Indrek Tallo.** Synthesis and characterization of new micro-mesoporous carbide derived carbon materials for high energy and power density electrical double layer capacitors. Tartu, 2015, 148 p.
147. **Heiki Erikson.** Electrochemical reduction of oxygen on nanostructured palladium and gold catalysts. Tartu, 2015, 204 p.
148. **Erik Anderson.** *In situ* Scanning Tunnelling Microscopy studies of the interfacial structure between Bi(111) electrode and a room temperature ionic liquid. Tartu, 2015, 118 p.
149. **Girinath G. Pillai.** Computational Modelling of Diverse Chemical, Biochemical and Biomedical Properties. Tartu, 2015, 140 p.
150. **Piret Pikma.** Interfacial structure and adsorption of organic compounds at Cd(0001) and Sb(111) electrodes from ionic liquid and aqueous electrolytes: an *in situ* STM study. Tartu, 2015, 126 p.
151. **Ganesh babu Manoharan.** Combining chemical and genetic approaches for photoluminescence assays of protein kinases. Tartu, 2016, 126 p.
152. **Carolin Siimenson**. Electrochemical characterization of halide ion adsorption from liquid mixtures at Bi(111) and pyrolytic graphite electrode surface. Tartu, 2016, 110 p.
153. **Asko Laaniste.** Comparison and optimisation of novel mass spectrometry ionisation sources. Tartu, 2016, 156 p.
154. **Hanno Evard.** Estimating limit of detection for mass spectrometric analysis methods. Tartu, 2016, 224 p.
155. **Kadri Ligi.** Characterization and application of protein kinase-responsive organic probes with triplet-singlet energy transfer. Tartu, 2016, 122 p.
156. **Margarita Kagan.** Biosensing penicillins' residues in milk flows. Tartu, 2016, 130 p.
157. **Marie Kriisa.** Development of protein kinase-responsive photoluminescent probes and cellular regulators of protein phosphorylation. Tartu, 2016, 106 p.
158. **Mihkel Vestli.** Ultrasonic spray pyrolysis deposited electrolyte layers for intermediate temperature solid oxide fuel cells. Tartu, 2016, 156 p.
159. **Silver Sepp**. Influence of porosity of the carbide-derived carbon on the properties of the composite electrocatalysts and characteristics of polymer electrolyte fuel cells. Tartu, 2016, 137p.
160. **Kristjan Haav**. Quantitative relative equilibrium constant measurements in supramolecular chemistry. Tartu, 2017, 158 p.

161. **Anu Teearu**. Development of MALDI-FT-ICR-MS methodology for the analysis of resinous materials. Tartu, 2017, 205 p.
162. **Taavi Ivan**. Bifunctional inhibitors and photoluminescent probes for studies on protein complexes. Tartu, 2017, 140 p.
163. **Maarja-Liisa Oldekop**. Characterization of amino acid derivatization reagents for LC-MS analysis. Tartu, 2017, 147 p.
164. **Kristel Jukk**. Electrochemical reduction of oxygen on platinum- and palladium-based nanocatalysts. Tartu, 2017, 250 p.
165. **Siim Kukk**. Kinetic aspects of interaction between dopamine transporter and *N*-substituted nortropane derivatives. Tartu, 2017, 107 p.
166. **Birgit Viira**. Design and modelling in early drug development in targeting HIV-1 reverse transcriptase and Malaria. Tartu, 2017, 172 p.
167. **Rait Kivi**. Allostery in cAMP dependent protein kinase catalytic subunit. Tartu, 2017, 115 p.
168. **Agnes Heering**. Experimental realization and applications of the unified acidity scale. Tartu, 2017, 123 p.
169. **Delia Juronen**. Biosensing system for the rapid multiplex detection of mastitis-causing pathogens in milk. Tartu, 2018, 85 p.
170. **Hedi Rahnel.** ARC-inhibitors: from reliable biochemical assays to regulators of physiology of cells. Tartu, 2018, 176 p.
171. **Anton Ruzanov.** Computational investigation of the electrical double layer at metal–aqueous solution and metal–ionic liquid interfaces. Tartu, 2018, 129 p.
172. **Katrin Kestav.** Crystal Structure-Guided Development of Bisubstrate-Analogue Inhibitors of Mitotic Protein Kinase Haspin. Tartu, 2018, 166 p.
173. **Mihkel Ilisson.** Synthesis of novel heterocyclic hydrazine derivatives and their conjugates. Tartu, 2018, 101 p.
174. **Anni Allikalt.** Development of assay systems for studying ligand binding to dopamine receptors. Tartu, 2018, 160 p.
175. **Ove Oll.** Electrical double layer structure and energy storage characteristics of ionic liquid based capacitors. Tartu, 2018, 187 p.
176. **Rasmus Palm.** Carbon materials for energy storage applications. Tartu, 2018, 114 p.